NASA MEMO 5-9-59L

NASA

MEMORANDUM

HYDRODYNAMIC CHARACTERISTICS OF TWO LOW-DRAG SUPERCAVITATING HYDROFOILS

By John R. McGehee and Virgil E. Johnson, Jr.

Langley Research Center
Langley Field, Va.

NATIONAL AERONAUTICS AND SPACE ADMINISTRATION
WASHINGTON
June 1959

NATIONAL AERONAUTICS AND SPACE ADMINISTRATION

MEMORANDUM 5-9-59L

HYDRODYNAMIC CHARACTERISTICS OF TWO LOW-DRAG SUPERCAVITATING HYDROFOILS

By John R. McGehee and Virgil E. Johnson, Jr.

SUMMARY

An experimental investigation has been conducted in Langley tank no. 2 to determine the hydrodynamic characteristics of two low-drag supercavitating hydrofoils operating in a range of cavitation numbers from 0 to approximately 6. The hydrofoils had aspect ratios of 1 and 3, and the sections were derived by assuming five terms in the vorticity-distribution expansion of the equivalent airfoil. The aspect-ratio-1 hydrofoil was also tested at zero cavitation number with two sets of end plates having depths of 3/8 and 1/4 chords.

Zero cavitation number was established by operating the hydrofoils near the water surface so that complete ventilation of the upper surfaces could be obtained. For those depths of submersion where complete ventilation was not obtained through vortex ventilation, two probes were used to introduce air to the upper surfaces of the hydrofoils and to induce complete ventilation. Data were obtained for a range of speeds from 20 to 80 fps, angles of attack from 2° to 20°, and ratios of depth of submersion to chord from 0 to 0.85.

The experimental results obtained from the aspect-ratio-1 and aspect-ratio-3, five-term hydrofoils were compared with a three-dimensional zero-cavitation-number theory. The theoretical and experimental values of lift and center of pressure for the aspect-ratio-1 hydrofoil were in agreement, within engineering accuracy, for the range of lift coefficients investigated. The theoretical drag coefficients were lower, by a constant amount, than the experimental drag coefficients. The theoretical expressions derived for the lift, drag, and center of pressure of the aspect-ratio-3 hydrofoil were in agreement, within engineering accuracy, with the experimental values. The theoretical and experimental drag coefficients of the aspect-ratio-3 five-term hydrofoil were lower than the theoretical drag coefficients computed for a comparable Tulin-Burkart hydrofoil.

INTRODUCTION

The existence of lifting surfaces with cavitating or ventilating characteristics superior to those of conventional airfoil sections is discussed in references 1 and 2. In reference 1, a linearized theory is presented for determining the characteristics of supercavitating two-dimensional hydrofoils of arbitrary section operating at zero cavitation number. A low-drag section was chosen in reference 1 by specifying two sine terms in the vorticity-distribution expansion of the equivalent airfoil, and then these two coefficients were adjusted so that the necessary conditions for high lift-drag ratios were satisfied. In reference 2, configurations were developed by choosing five terms in the vorticity-series expansion and then adjusting the coefficients exactly as was done in reference 1. These configurations (ref. 2) were theoretically better than those of reference 1. The number of terms selected in reference 2 for the analysis were three and five. In reference 3, a three-dimensional theory was developed for predicting the forces on supercavitating hydrofoils operating at a finite depth and zero cavitation number.

The purpose of the present experimental investigation was to verify the three-dimensional theory of reference 3 and to compare the lift-drag ratios of the five-term section with those of the two-term section derived by Tulin and Burkart. Aspect-ratio-1 and aspect-ratio-3 five-term hydrofoils were tested with the upper surfaces completely ventilated and thus operating at essentially zero cavitation number. These hydrofoils were also tested at cavitation numbers greater than zero. In addition, the aspect-ratio-1 hydrofoil was tested with end plates of 3/8- and 1/4-chord depths at essentially zero cavitation number.

SYMBOLS

A	aspect ratio
A_1	coefficient of first term in sine-series expansion of airfoil vorticity distribution
c	chord of hydrofoil, in.
C_D	total drag coefficient, $\frac{D}{qS}$
$C_{f,h}$	friction-drag coefficient for hydrofoil

$C_{f,s}$	friction-drag coefficient for strut as a function of spray-thickness—chord ratio
$C_{f,t}$	total friction-drag coefficient, $C_{f,h} + C_{f,s}$
C_L	total lift coefficient, $\frac{L}{qS}$
$C_{L,d}$	design lift coefficient at $\alpha = 0$
D	total drag, lb
d	leading-edge depth of submersion, in.
L	total lift, lb
p_∞	pressure at infinity, lb/sq ft
p_v	fluid vapor pressure, lb/sq ft
q	free-stream dynamic pressure, $\frac{\rho V^2}{2}$, lb/sq ft
S	area, sq ft
V	speed of advance, fps
x	distance from leading edge along X-axis, in.
x_{cp}	distance from leading edge to center of pressure, in.
y	distance along Y-axis, in.
α	geometric angle of attack, deg
α_c	angle of attack due to camber, deg
$\alpha_{c,\infty}$	angle of attack due to camber at infinite depth, deg
δ	spray thickness, in.
ϕ	angle between spray and horizontal, deg

ρ mass density, slugs/cu ft

σ cavitation number, $\frac{p_\infty - p_v}{q}$

MODELS

The greatest advantage of the low-drag supercavitating hydrofoils is obtained at low angles of attack, which result in the formation of thin cavities. Because the hydrofoils are designed to operate within a cavity, the shape of the upper surface is arbitrary as long as it does not interfere with the formation of the cavity. The hydrofoils tested in this investigation had flat upper surfaces and were designed as thin as structurally feasible. Since the principal purpose of this investigation was to verify the three-dimensional theory of reference 3, the models were selected to represent appreciably different aspect ratios and cambers.

The lower profiles (fig. 1) were computed from the following equation (ref. 2):

$$y/c = \frac{A_1}{315}\left[210(x/c) - 2{,}240(x/c)^{3/2} + 12{,}600(x/c)^2 - 30{,}912(x/c)^{5/2} + 35{,}840(x/c)^3 - 15{,}360(x/c)^{7/2}\right]$$

where for the aspect-ratio-1 hydrofoil

$$A_1 = 0.150 \qquad \left(C_{L,d} = 0.3927\right)$$

and for the aspect-ratio-3 hydrofoil

$$A_1 = 0.075 \qquad \left(C_{L,d} = 0.1964\right)$$

Coordinates for the lower surfaces are shown in figure 1. The aspect-ratio-1 hydrofoil had a chord and a span of 7.071 inches and was square in plan form. The aspect-ratio-3 hydrofoil had a chord of 4.083 inches and a span of 12.247 inches and was rectangular in plan form. Both hydrofoils had a plan-form area of 50 square inches.

The end plates for the aspect-ratio-1 hydrofoil (fig. 2) were designed to attach perpendicular to and flush with the upper surface of the hydrofoil and to extend below the chord to depths of 3/8 chord and

1/4 chord. They had sharp leading and bottom edges and a blunt trailing edge. Photographs of the model configurations are given in figure 3.

The strut section was an NACA 66_1-012 section and is shown in figure 4 with a table of coordinates. The strut had a 4-inch chord and was 19 inches long. The strut was mounted perpendicular to and in the center of the spans of the upper surfaces of the hydrofoils. The intersection of the strut and the upper surfaces of the hydrofoils was without fillets.

The hydrofoils, end plates, and strut were made of stainless steel, heat-treated for additional strength, and polished to a smooth finish.

APPARATUS AND PROCEDURE

The tests were conducted on the Langley tank no. 2 towing carriage. Lift, drag, and pitching moment were measured with existing strain-gage balances which independently determined forces and moments. The pitching moments were measured about an arbitrary point above the hydrofoil and the data thus obtained were used to calculate the moments about the leading edge.

The forces and moments were measured at constant speeds, depths of submersion, and angles of attack. These forces and moments include those contributed by the strut. The depth of submersion was defined as the vertical distance between the leading edge of the hydrofoil and the undisturbed water surface. In order to facilitate the comparison of the data between the aspect-ratio-1 and aspect-ratio-3 hydrofoils, the depths of submersion investigated were such that depth-of-submersion—chord ratios for the two hydrofoils were the same. The angle of attack was defined as the angle between the reference lines of the models and the free-water surface.

Zero cavitation number was obtained by operating the hydrofoils at small depths of submersion and establishing complete ventilation of the upper surfaces. The zero-cavitation-number tests were made on all model configurations for a range of angles of attack from the minimum angle at which complete ventilation could be established to 20°, speeds from 50 to 80 fps, and a depth-of-submersion—chord ratio of 0.071. The aspect-ratio-1 and aspect-ratio-3 hydrofoils were also tested at angles of attack from 8° to 20°, speeds from 50 to 80 fps, and depth-of-submersion—chord ratios from 0 to 0.85. Due to the nature of the test equipment, exact speeds could not be preset but were accurately measured. Therefore, the data were plotted against speed and faired values are presented for speeds at 10-foot-per-second intervals. Also, because of structural deflections, the data were obtained at values of angle of

attack other than those proposed. Therefore, the data were plotted against angle of attack and faired values are presented for angles of attack of 2° increments.

For those depths of submersion and angles of attack at which complete ventilation could not be obtained through the process of vortex ventilation (ref. 4), two probes were used to introduce air to the upper surfaces of the hydrofoils and thus induce complete ventilation. These probes had a long trailing cavity at relatively low speeds and supplied large quantities of air to the upper surfaces of the hydrofoils. The probes were located on each side of the strut, $1\frac{1}{2}$ inches outboard (fig. 5), to prevent unsymmetrical ventilation and loading. During the earlier portion of the tests, the probes were introduced into the flow at the 1/4-chord points of the hydrofoils. As the testing progressed to the greater depths of submersion, it was necessary to introduce the probes nearer the leading edges to establish complete ventilation. The procedure normally employed for inducing ventilation by using the probes was to accelerate the model to test speed, introduce the probes until ventilation was established, withdraw the probes, and then record data. After ventilation was established and the probes removed, the ventilation was maintained by atmospheric air which entered in the rearward portion of the cavity. In some instances the probes had to be located slightly forward of the leading edges with the bottom of the probes below the leading edges. When this location of the probes was not effective, the probes were left in the flow during the acceleration to speed and if ventilation occurred the probes were removed. Since the primary objective of the tests was to determine the forces and moments at zero cavitation number, any method that established complete ventilation with the probes removed was satisfactory.

The thickness δ and the spray angle ϕ were measured by the spray-thickness gage. (See fig. 6.) A description of the operation of this instrument is presented in reference 3.

Tests were made at finite cavitation numbers on the aspect-ratio-1 and aspect-ratio-3 hydrofoils at a depth-of-submersion—chord ratio of 0.85, angles of attack from 4° to 20°, and speeds from 20 to 80 fps.

ACCURACY

The changes in angle of attack due to structural deflections of the balances and supporting system were determined during the calibration of the balances and the test data were corrected accordingly.

The estimated accuracy of the test measurements was as follows:

Angle of attack, deg	±0.1
Speed, fps	±0.2
Depth of submersion, in.	±0.1
Lift, lb	±15
Drag, lb	±7
Moment, ft-lb	±6
Spray thickness, in.	±0.05
Spray angle, deg	±1.5

The forces and moments were converted to the usual aerodynamic coefficient form by using a measured value of the water density of 1.944 slugs/cu ft. The kinematic viscosity measured during the tests was 1.07×10^{-5} ft^2/sec. Thus, for the range of velocities investigated, the Reynolds number based on the chord ranged from 1.02×10^6 to 2.82×10^6. Cavitation numbers were computed using values of barometric pressure and water temperature which were obtained daily.

RESULTS AND DISCUSSION

Presentation of Results

Zero cavitation number.- The lift, drag, and pitching moment about the leading edge for the aspect-ratio-1 hydrofoil, the aspect-ratio-3 hydrofoil, and the aspect-ratio-1 hydrofoil with end plates are presented in figures 7, 8, and 9, respectively. The data were plotted as a function of angle of attack with speed as a parameter. The open symbols represent data obtained where complete ventilation occurred through vortex ventilation. The solid symbols represent data obtained by using the probes to induce complete ventilation.

The minimum angle of attack at which complete ventilation occurred through vortex ventilation varied with depth of submersion, speed, aspect ratio, and the addition of end plates. Complete ventilation through vortex ventilation was only established at small depths of submersion. The disparity shown in figure 7(a) for angles of attack of 10°, 12°, and 14° and a velocity of 50 fps may have been caused by a small change in depth of submersion due to a surge in the towing tank. The minimum angle of attack at which complete ventilation occurred increased with increasing depth of submersion. For a given depth of submersion, the minimum angle of attack for complete ventilation decreased with increasing speed. Ventilation of the upper surface of these hydrofoils depends upon the fully wetted characteristics. For a given angle of attack, the hydrofoil with the thinner section and smaller camber (aspect ratio 3) is at a higher effective angle of attack in the fully

wetted condition than the hydrofoil with the thicker section and larger camber (aspect ratio 1). Therefore, the decrease in the minimum angle of attack for complete ventilation with increasing aspect ratio, as indicated in figures 7 and 8, also includes the effects of thickness and camber. The addition of end plates to the aspect-ratio-1 hydrofoil (fig. 9) caused an increase in the minimum angle of attack for complete ventilation. It should be noted that the effect of end plates on the minimum angle of attack for complete ventilation through vortex ventilation was determined solely for a depth of submersion of 0.5 inch.

The minimum angle of attack at which complete ventilation could be induced varied with depth of submersion and aspect ratio in the same manner as that for complete ventilation through vortex ventilation. The addition of end plates to the aspect-ratio-1 hydrofoil resulted in a decrease in the minimum angle of attack at which complete ventilation could be induced. It may be noted that this is contrary to the results obtained with vortex ventilation. With the addition of end plates to the aspect-ratio-1 hydrofoil there was no single discrete vortex formed. Even though the addition of end plates did result in an increase in the effective angle of attack, the supply of air necessary to establish complete ventilation through vortex ventilation could not reach the upper surface of the hydrofoil. On the other hand when a path for the air was provided, through the use of probes, ventilation could be established at lower angles of attack. The scope of the investigation was such that the effect of speed on the minimum angle of attack for induced ventilation could not be established. Complete ventilation is shown for all model configurations in figure 10.

Finite cavitation number.- The lift coefficients and drag coefficients obtained from the finite-cavitation-number tests are presented in figures 11 and 12. The dashed curves shown in these figures are extrapolations of the experimental curves to the theoretical values computed for zero cavitation number. The arrows indicate the cavitation numbers at which cavitation was first observed at the leading and trailing edges of the hydrofoils.

For the aspect-ratio-1 hydrofoil, the lift coefficients for a given angle of attack were approximately constant for the higher range of cavitation numbers. In general, for the lower range of cavitation numbers the lift coefficients decreased with decreasing cavitation number. The lift coefficients computed for zero cavitation number were less than the lift coefficients obtained experimentally at cavitation numbers greater than zero for angles of attack of 12°, 16°, and 20°. The lift coefficients computed for zero cavitation number and an angle of attack of 8° were not smaller than those obtained experimentally. At this angle of attack, the upper surface of the hydrofoil was always wetted and therefore contributed a negative lift component to the total lift. The calculated value for zero cavitation number assumed that the upper

surface was in a cavity and had no effect on the lifting characteristics. The drag coefficients generally increased with decreasing cavitation numbers for the higher range of cavitation numbers and decreased with decreasing cavitation numbers for the lower range of cavitation numbers.

For the aspect-ratio-3 hydrofoil, the lift coefficients for all angles of attack were essentially constant for the higher range of cavitation numbers. For the lower range of cavitation numbers, the lift coefficients generally decreased with decreasing cavitation number. The theoretical lift coefficients computed for angles of attack of 8°, 12°, 16°, and 20° and zero cavitation number were lower than those determined experimentally. At an angle of attack of 4°, the upper surface of the hydrofoil was always wetted and as explained previously the theoretical lift coefficient, computed for zero cavitation number, was larger than the lift coefficients determined experimentally. The drag coefficients showed apparent dispersion beyond the range of the estimated accuracy, but evidently they are approximately constant for the higher range of cavitation numbers. For the lower range of cavitation numbers, the drag coefficients decreased with decreasing cavitation number.

Underwater photographs of the aspect-ratio-1 and aspect-ratio-3 hydrofoils operating at cavitation numbers greater than zero are shown in figure 13. These photographs, which were taken with the hydrofoils at an angle of attack of 20° and a ratio of depth of submersion to chord of 0.85, may be correlated with the data in figures 11 and 12.

End-plate effects.- The lift coefficient, lift-drag ratio, and center-of-pressure—chord ratio for the aspect-ratio-1 hydrofoil, aspect-ratio-1 hydrofoil with small end plates, aspect-ratio-1 hydrofoil with large end plates, and aspect-ratio-3 hydrofoil are presented in figure 14 for a ratio of depth of submersion to chord of 0.071. The lift coefficients of the hydrofoil with the small end plates were approximately 33 percent greater than those of the hydrofoil with no end plates; whereas, the lift coefficients of the hydrofoil with the large end plates were approximately 39 percent greater than those of the hydrofoil with no end plates. Also, the lift-drag ratios of both the end-plate configurations were greater than those of the basic configuration.

Spray thickness.- The spray-thickness—chord ratios for the present models are shown plotted in figure 15 and the spray-thickness data obtained at angles of attack of 16° and 20° are compared in figure 16 with similar data obtained for an aspect-ratio-1 flat plate. The spray thickness is the same as the depth of submersion for a flat plate at an angle of attack of 0° and only slightly greater than the depth of submersion for a cambered section. Therefore, the curves through the experimental values of spray-thickness—chord ratio were drawn with depth-of-submersion—chord ratios at 0° angle of attack as end points. For both hydrofoils, at all depths of submersion, the spray thickness

increased with increasing angle of attack. The spray thickness of the aspect-ratio-3 hydrofoil increased at a greater rate with increasing angle of attack than that of the aspect-ratio-1 hydrofoil. It may be noted in figure 16 that an appreciable change in camber results in a negligible change in spray thickness, whereas a change in aspect ratio from 1 to 3 does produce a significant change. Qualitatively, this may be explained rather simply. If the hydrofoil is replaced by a horseshoe vortex system and a distribution of sources, the linearized location of the stagnation line at midspan may be obtained. Increases in the bound vorticity increase the slopes of the forward stagnation line which depresses the elevation of the stagnation line with respect to the hydrofoil leading edge and thus the spray thickness is increased. Greatest effects of the bound vorticity are obtained when most of the vorticity is near the leading edge, as is the vorticity due to angle of attack. Camber vorticity which is concentrated more rearward does not have a proportionally large effect on the depression of the stagnation-line elevation below that of the hydrofoil leading edge. The trailing vorticity tends to raise the stagnation-line elevation and thus decreases the spray thickness. The trailing vortices have the greatest influence on the location of the stagnation line at small aspect ratios; this influence decreases with increase in aspect ratio.

Comparison of Experimental Results With Theory

The theoretical lift coefficient, drag coefficient, center of pressure, and spray angle were computed from equations derived from the three-dimensional theory in reference 3. The experimental drag data were not corrected for the frictional drag of the hydrofoils or strut; therefore, computed values of the frictional drag coefficient for the strut and one side of the hydrofoils were added to the theoretical drag coefficients. The friction-drag coefficients for the strut and for one surface of the hydrofoils were computed from the following equations which were derived from Schoenherr's equation using average values of Reynolds number:

For aspect-ratio-3 hydrofoil:

$$C_{f,t} = C_{f,h} + C_{f,s} = 0.0041 + 0.0026 \frac{\delta}{c}$$

For aspect-ratio-1 hydrofoil:

$$C_{f,t} = C_{f,h} + C_{f,s} = 0.0038 + 0.0046 \frac{\delta}{c}$$

Spray angles.- The variations of the theoretical and experimental spray angles with depth-of-submersion—chord ratio for angles of attack

were similar for both the aspect-ratio-1 and aspect-ratio-3 hydrofoils. (See fig. 17.) The aspect-ratio-1 hydrofoil showed good agreement between theory and experiment for depth-of-submersion—chord ratios greater than 0.08. For depth-of-submersion—chord ratios less than 0.08, the experimental values were generally lower than the theoretical values. The agreement between theory and experiment was not as good for the aspect-ratio-3 hydrofoil as it was for the aspect-ratio-1 hydrofoil.

The theoretical method for obtaining the spray angle assumes that the spray angles are small. Thus, the theory is expected to be in error for very shallow depths where the spray angle is large and a more refined method of calculating the location of the cavity upper surface is needed. The method should include the effects of depth, angle of attack, camber, and aspect ratio. Hydrofoils designed with spray angles calculated by the method of reference 3 can actually operate ventilated at angles of attack slightly less than those predicted by theory.

Lift coefficients.- The experimental and theoretical lift coefficients are presented as a function of depth-of-submersion—chord ratio with angle of attack as a parameter in figure 18. The theoretical lift coefficients are in excellent agreement with the experimental lift coefficients for depth-of-submersion—chord ratios above approximately 0.071 and for all angles of attack where complete ventilation was obtained.

It was pointed out in reference 3 that the theory would be least accurate for very small depths of submersion. The reason for this inaccuracy is that the effect of camber is determined by assuming that the spray thickness and the depth of submersion are the same and that the spray angle is small. These assumptions are not valid for the smaller depths of submersion of the present investigation. Thus, the aspect-ratio-3 model with less camber than the aspect-ratio-1 model would be expected to have less discrepancy between theory and experiment at shallow depths. It may be noted that the discrepancy in the theory can be considerably improved if the value of $\frac{\alpha_c}{\alpha_{c,\infty}}$ in reference 3 is determined for the true value of δ/c instead of for d/c.

Drag coefficients.- The experimental and theoretical drag coefficients are presented as a function of depth-of-submersion—chord ratio with angle of attack as a parameter in figure 19. The theoretical drag coefficients computed for the aspect-ratio-1 hydrofoil were lower than the experimental drag coefficients at all angles of attack and depth-of-submersion—chord ratios. The linearized theory is applicable to any surface configuration (with positive lower surface pressures) as long as the angle of attack and camber are small. The aspect-ratio-1 hydrofoil tested in the present investigation had a considerable amount of camber. Even though the theory appeared to be applicable for predicting the lift, the drag predicted by the theory was lower than that obtained

experimentally possibly because of the large camber of the hydrofoil. The pressure-distribution curve which produces a given lift may have a large variation in shape. When these pressures act on a surface with large curvature, the drag coefficient will be extremely sensitive to the shape of the pressure-distribution curve. In the case of the aspect-ratio-1 hydrofoil, only a small rearward movement of the theoretical location of maximum pressure will significantly increase the drag coefficient with little effect on the lift coefficient.

Good agreement was obtained between theory and experiment for the aspect-ratio-3 hydrofoil throughout the ranges of angle of attack and depth-of-submersion—chord ratios investigated.

Centers of pressure.- In figure 20, theoretical and experimental center-of-pressure—chord ratios are presented as a function of angle of attack with depth-of-submersion—chord ratio as a parameter. For both the aspect-ratio-1 and aspect-ratio-3 hydrofoils, the theoretical center-of-pressure distances rearward of the leading edge did not change significantly with increase in depth of submersion. Similarly, the experimental center-of-pressure distances for both hydrofoils did not change appreciably with increasing depth of submersion.

The experimental center-of-pressure—chord ratios for the aspect-ratio-1 hydrofoil ranged from 8 to 13 percent greater than the theoretical ratios. The variation with angle of attack of both the theoretical and experimental center-of-pressure—chord ratios was essentially the same.

The experimental center-of-pressure—chord ratios for the aspect-ratio-3 hydrofoil were about 1 to 10 percent greater than the theoretical ratios. The variation of the experimental center-of-pressure—chord ratios with increasing angles of attack was less than that of the theoretical ratios.

It was suggested in reference 3 that the resultant crossflow component of force is probably located on the rearward portion of hydrofoils such as the five-term section rather than at the midchord as in the case for a flat plate. The curves shown in figure 20 were calculated using the midchord for the crossflow force vector; however, it may be noted that selection of a point closer to the trailing edge for the application of the crossflow vector will lead to better agreement with the experimental data.

Lift-drag ratios.- Theoretical and experimental lift-drag ratios for depth-of-submersion—chord ratios of 0.071 and 0.566 are shown in figure 21. The lift-drag ratios are plotted as a function of lift coefficient with angle of attack as a parameter. The theoretical and experimental lift-drag ratios for both the aspect-ratio-1 and aspect-ratio-3

hydrofoils were higher at the smaller depth-of-submersion—chord ratio than they were at the larger depth-of-submersion—chord ratio.

The experimental lift-drag ratios for the aspect-ratio-1 hydrofoil were lower than the theoretical values at all angles of attack. This was to be expected since the drag of the aspect-ratio-1 hydrofoil was higher than the drag predicted by the theory and the lift was approximately the same as that predicted by theory.

There was very good agreement between the theoretical and experimental lift-drag ratios for the aspect-ratio-3 hydrofoil at the higher angles of attack. As was the case with the aspect-ratio-1 hydrofoil, the experimental lift-drag ratios became, in general, increasingly lower than the theoretical ratios as the angle of attack decreased. The greater decrease in the experimental lift-drag ratio shown for an angle of attack of 2° and a depth-of-submersion—chord ratio of 0.071 was due to the fact that only partial ventilation could be established at this angle of attack.

Comparison of Five-Term-Section Hydrofoil With Tulin-Burkart Two-Term-Section Hydrofoil

Theoretical drag coefficients were computed for an aspect-ratio-3 hydrofoil with a Tulin-Burkart (two-term) section by using the zero-cavitation-number three-dimensional theory of reference 3. The drag coefficients for an aspect-ratio-3 Tulin-Burkart hydrofoil were computed by finding the value of A_1 that would produce a lift coefficient equal to the experimentally determined lift coefficient of the aspect-ratio-3 five-term hydrofoil at an angle of attack of 4° and a depth-of-submersion—chord ratio of 0.071. The calculated lift coefficients for the Tulin-Burkart section $(A_1 = 0.094)$ were found to agree with the experimentally obtained values for the aspect-ratio-3 hydrofoil for all angles of attack up to 20°. This value of A_1 (that is, 0.094) was then used in the computation of the three-dimensional theoretical drag coefficients. Comparisons of these drag coefficients are made in figure 22. The theoretical drag coefficients of the five-term hydrofoil were about 10 percent lower than those of the Tulin-Burkart hydrofoil. The experimental drag coefficients for the five-term hydrofoil were in good agreement with the theoretical drag coefficients for the five-term hydrofoil at the higher lift coefficients. As the lift coefficient decreases, the experimental values are above the theoretical values but still lower than those of the Tulin-Burkart hydrofoil.

CONCLUSIONS

The results of this investigation led to the following conclusions:

1. The theoretical and experimental values of lift and center of pressure for the aspect-ratio-1 hydrofoil, operating at zero cavitation number and finite depth of submersion, are in agreement within engineering accuracy. For the range of lift coefficients investigated the theoretical drag is lower, by a constant amount, than the experimental drag.

2. The theoretical expressions derived for the lift, drag, and center of pressure of the aspect-ratio-3 hydrofoil, operating at zero cavitation number and finite depth of submersion, are in agreement with the experimental values, within engineering accuracy.

3. The theoretical and experimental drag coefficients of the aspect-ratio-3 five-term hydrofoil are lower than the theoretical drag coefficients computed for a comparable Tulin-Burkart hydrofoil.

Langley Research Center,
National Aeronautics and Space Administration,
Langley Field, Va., February 12, 1959.

REFERENCES

1. Tulin, M. P., and Burkart, M. P.: Linearized Theory for Flows About Lifting Foils at Zero Cavitation Number. Rep. C-638, David W. Taylor Model Basin, Navy Dept., Feb. 1955.

2. Johnson, Virgil E., Jr.: Theoretical Determination of Low-Drag Supercavitating Hydrofoils and Their Two-Dimensional Characteristics at Zero Cavitation Number. NACA RM L57G11a, 1957.

3. Johnson, Virgil E., Jr.: Theoretical and Experimental Investigation of Abitrary Aspect Ratio, Supercavitating Hydrofoils Operating Near the Free Water Surface. NACA RM L57I16, 1957.

4. Wadlin, Kenneth L., Ramsen, John A., and Vaughn, Victor L., Jr.: The Hydrodynamic Characteristics of Modified Rectangular Flat Plates Having Aspect Ratios of 1.00, 0.25, and 0.125 and Operating Near a Free Water Surface. NACA Rep. 1246, 1955. (Supersedes NACA TN 3079 by Wadlin, Ramsen, and Vaughan and NACA TN 3249 by Ramsen and Vaughan.)

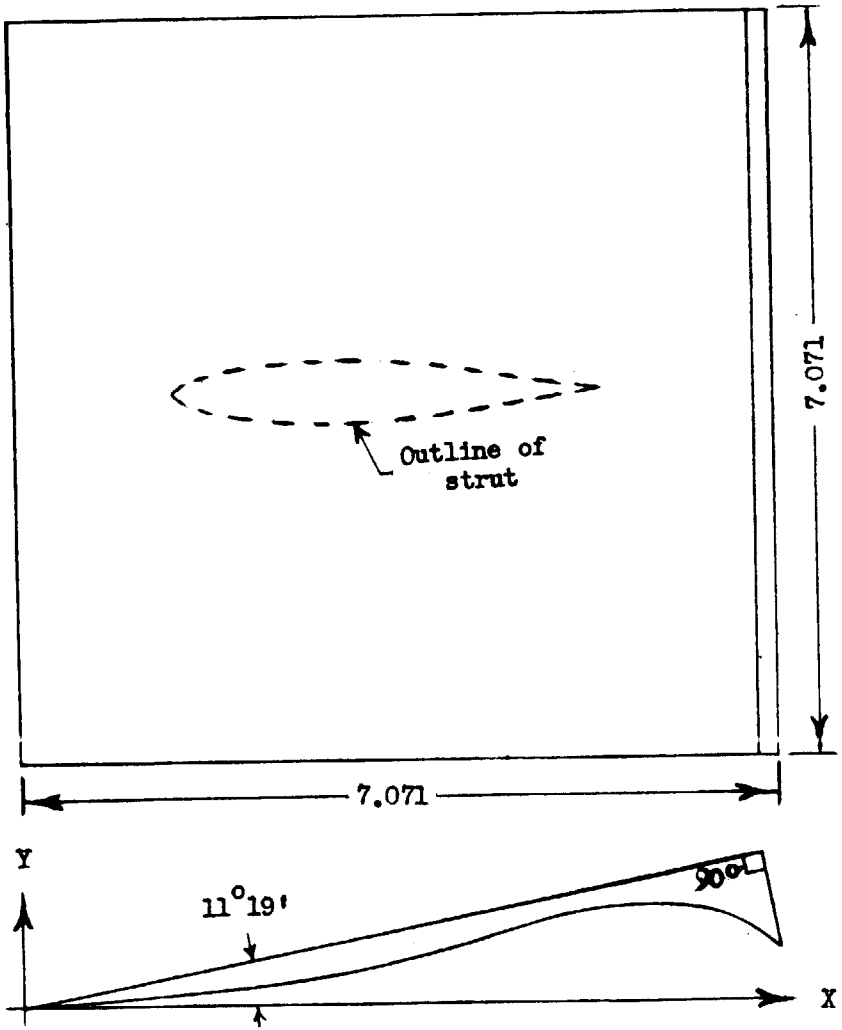

Table of coordinates for lower surface

x, in.	y, in.
0	0
0.177	0.006
0.354	0.013
0.707	0.032
1.414	0.082
2.121	0.153
2.475	0.199
2.828	0.260
3.182	0.330
3.536	0.407
3.889	0.491
4.243	0.582
4.596	0.670
4.950	0.747
5.303	0.809
5.657	0.843
5.810	0.846
6.010	0.839
6.364	0.785
6.718	0.669
7.071	0.465

(a) Aspect-ratio-1 hydrofoil.

Figure 1.- Model configurations. (All dimensions are in inches.)

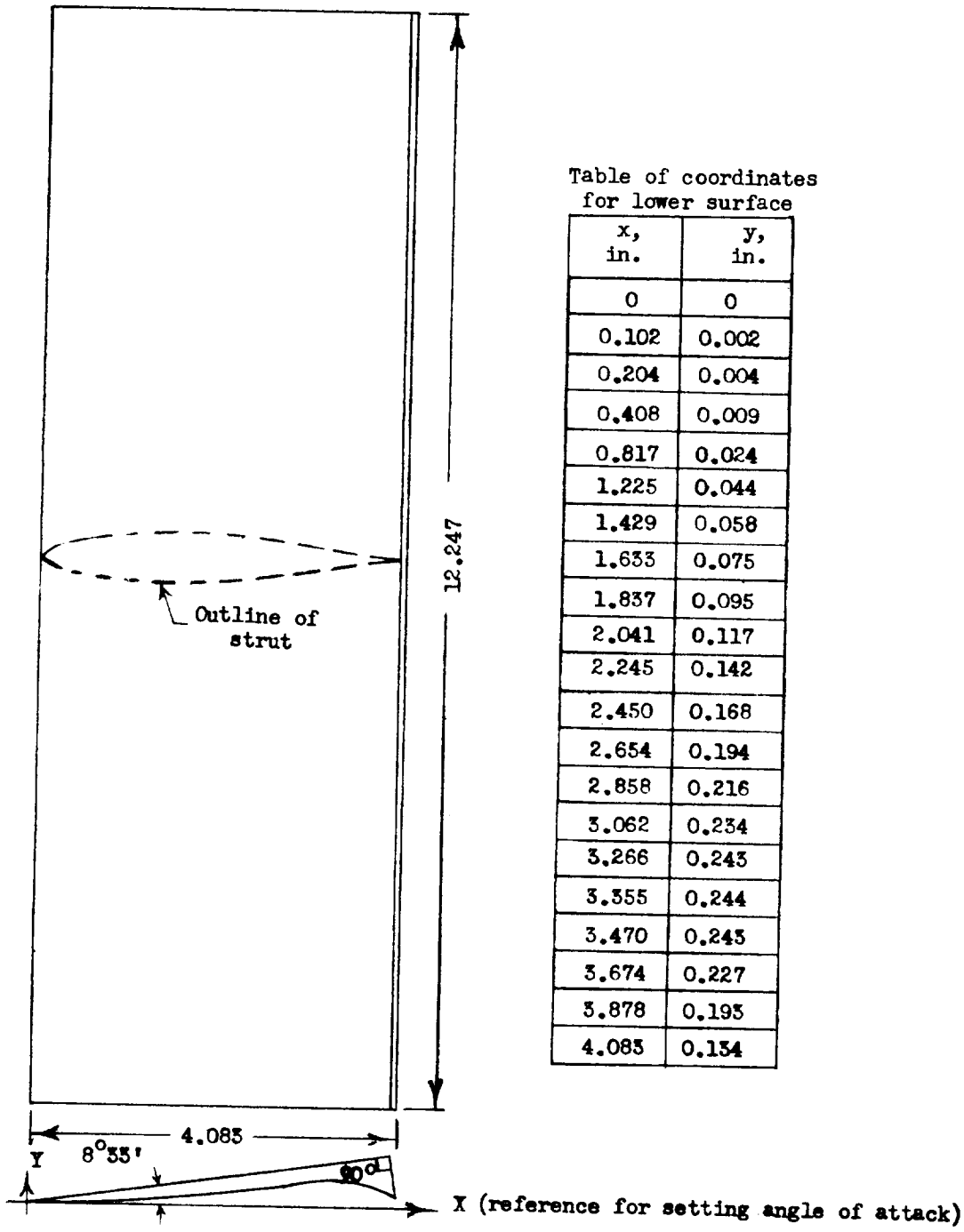

Table of coordinates for lower surface

x, in.	y, in.
0	0
0.102	0.002
0.204	0.004
0.408	0.009
0.817	0.024
1.225	0.044
1.429	0.058
1.633	0.075
1.837	0.095
2.041	0.117
2.245	0.142
2.450	0.168
2.654	0.194
2.858	0.216
3.062	0.234
3.266	0.243
3.355	0.244
3.470	0.243
3.674	0.227
3.878	0.193
4.083	0.154

(b) Aspect-ratio-3 hydrofoil.

Figure 1.- Concluded.

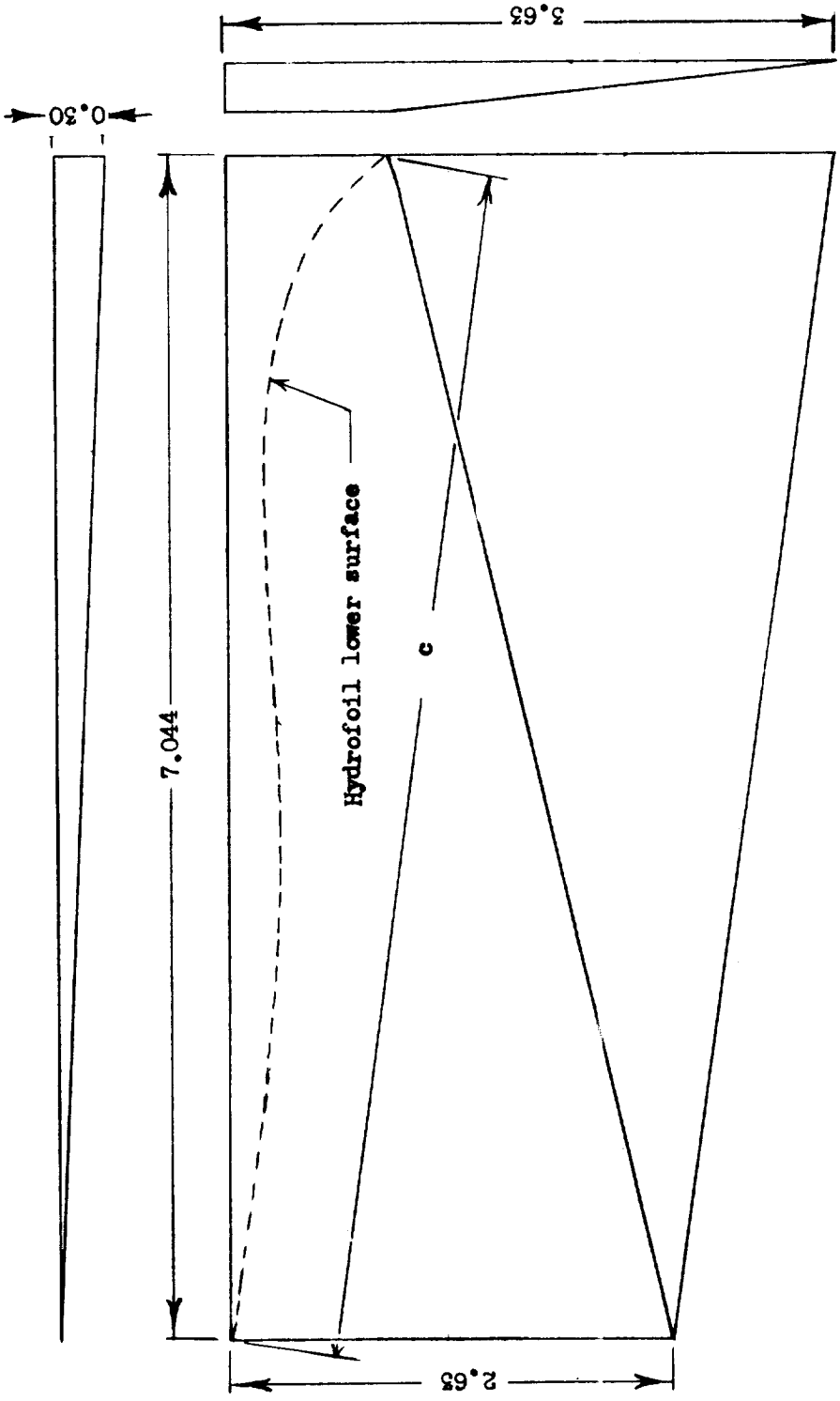

(a) Large end plates.

Figure 2.- End plates for aspect-ratio-1 hydrofoil. (All dimensions are in inches.)

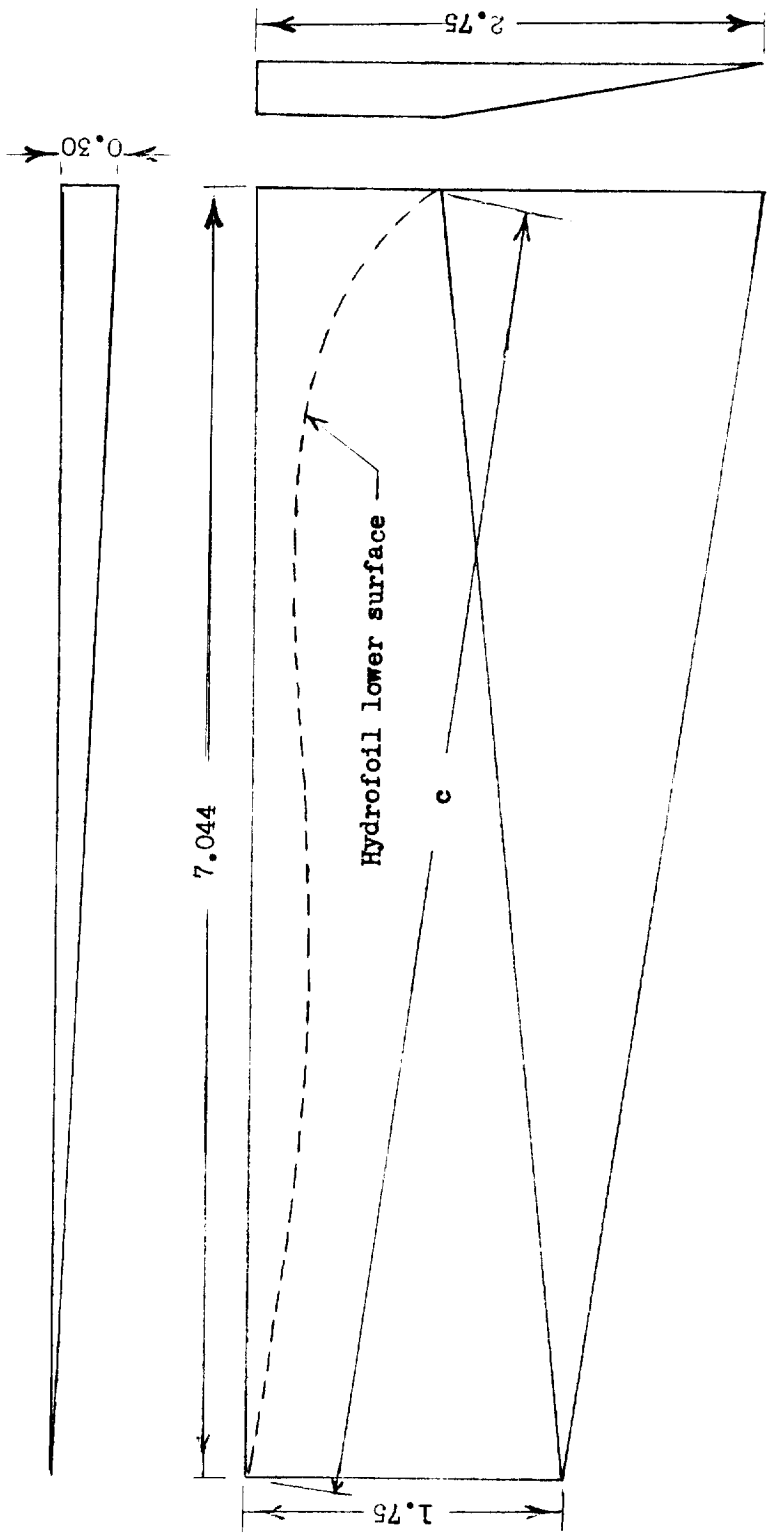

(b) Small end plates.

Figure 2.- Concluded.

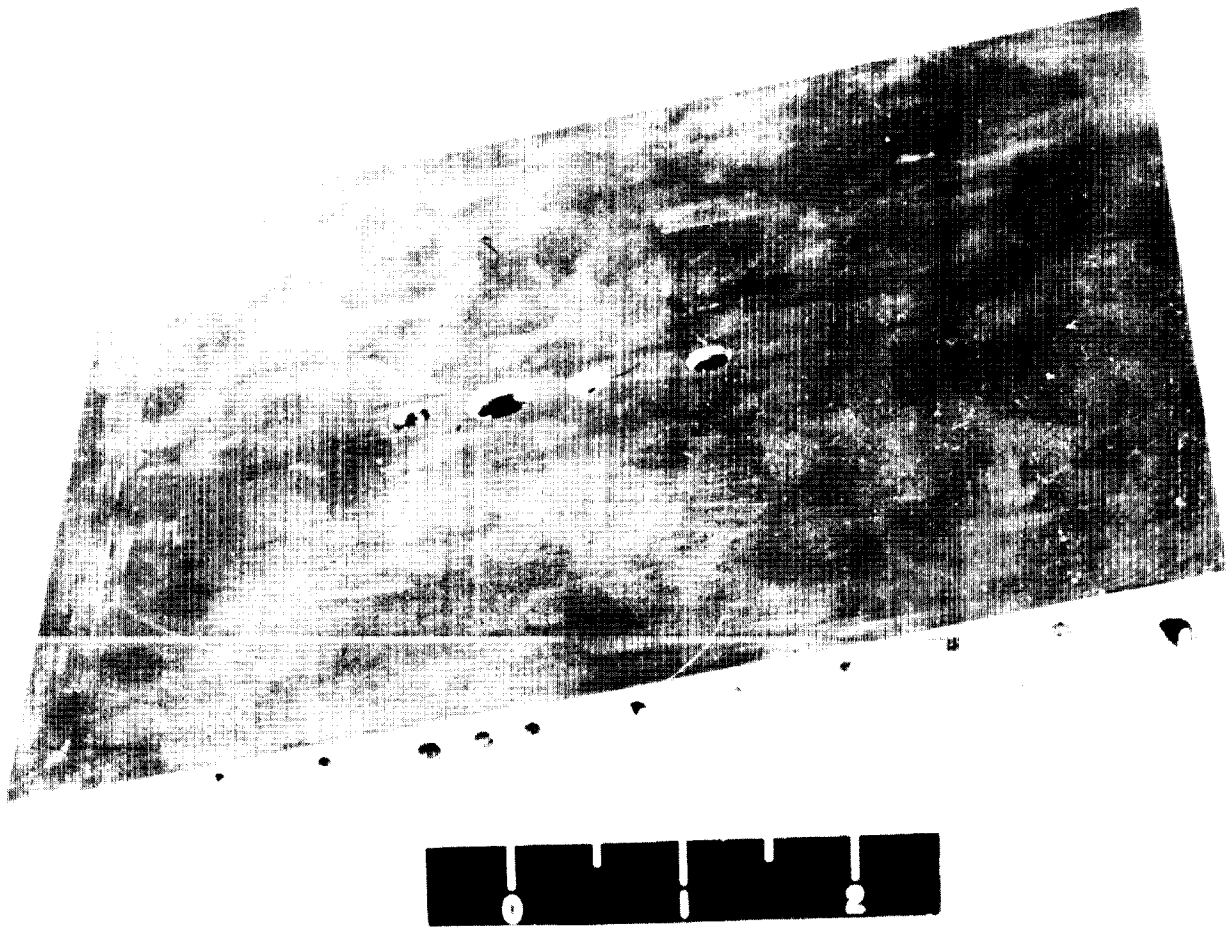

(a) Aspect-ratio-1 hydrofoil. L-59-200

Figure 3.- Photographs of model configurations.

(b) Aspect-ratio-3 hydrofoil. L-59-201

Figure 3.- Continued.

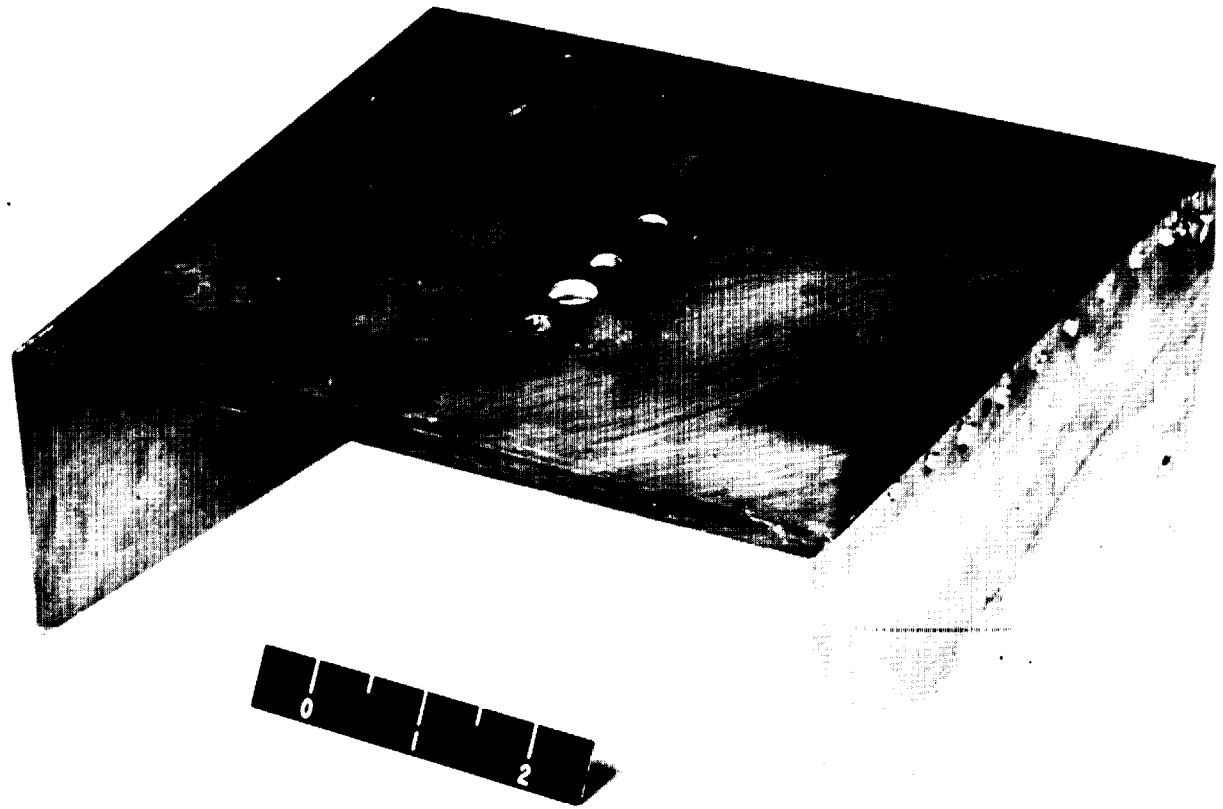

(c) Aspect-ratio-1 hydrofoil with large end plates. L-59-202

Figure 3.- Continued.

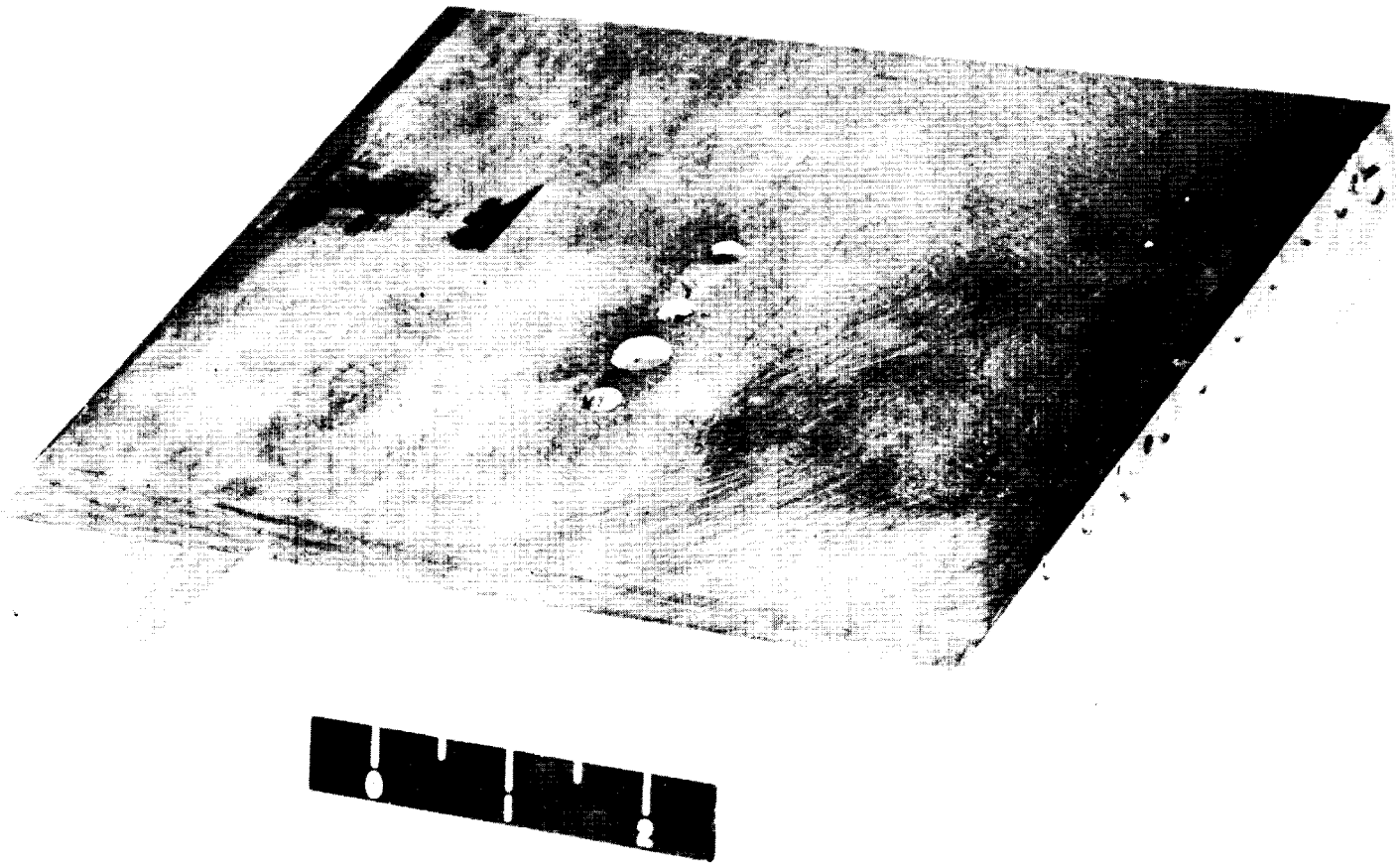

(d) Aspect-ratio-1 hydrofoil with small end plates. L-59-203

Figure 3.- Concluded.

x, in.	y, in.
0	0
.05	.019
.10	.049
.20	.083
.30	.118
.40	.151
.60	.181
.80	.205
1.00	.224
1.20	.233
1.40	.239
1.60	.240
1.80	.238
2.00	.232
2.20	.223
2.40	.210
2.60	.192
2.80	.169
3.00	.140
3.20	.122
3.40	.100
3.60	.072
3.80	.054
4.00	0

Figure 4.- Hydrofoil strut section (NACA 66_1-012 section).

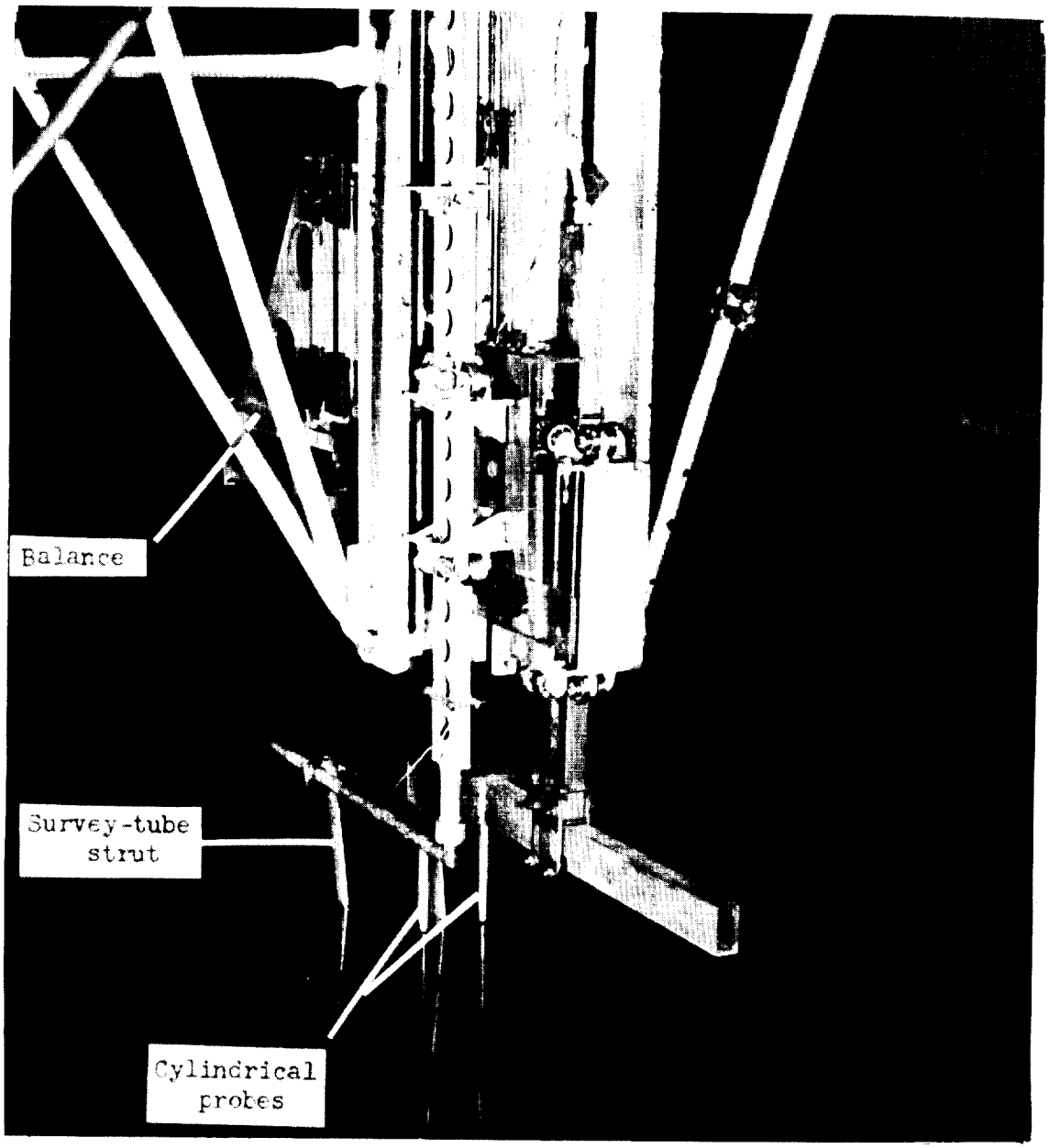

Figure 5.- Photograph of test setup. L-59-204

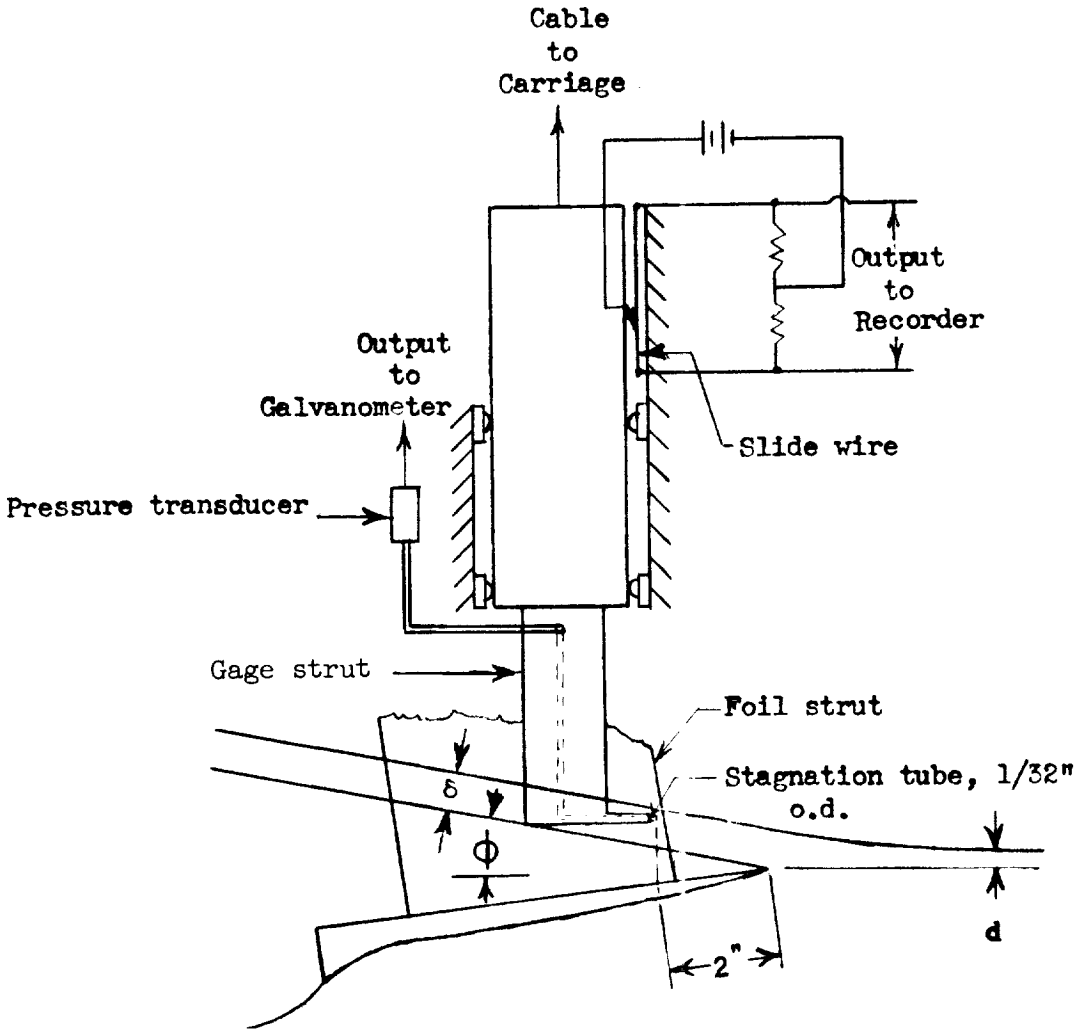

(a) Side elevation.

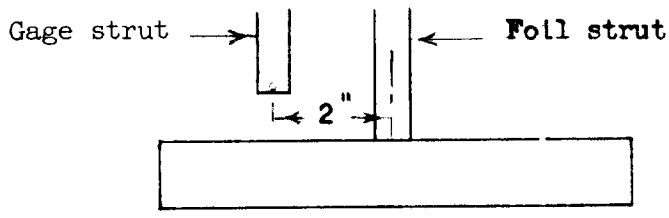

(b) Front elevation.

Figure 6.- Schematic drawing of spray-thickness gage.

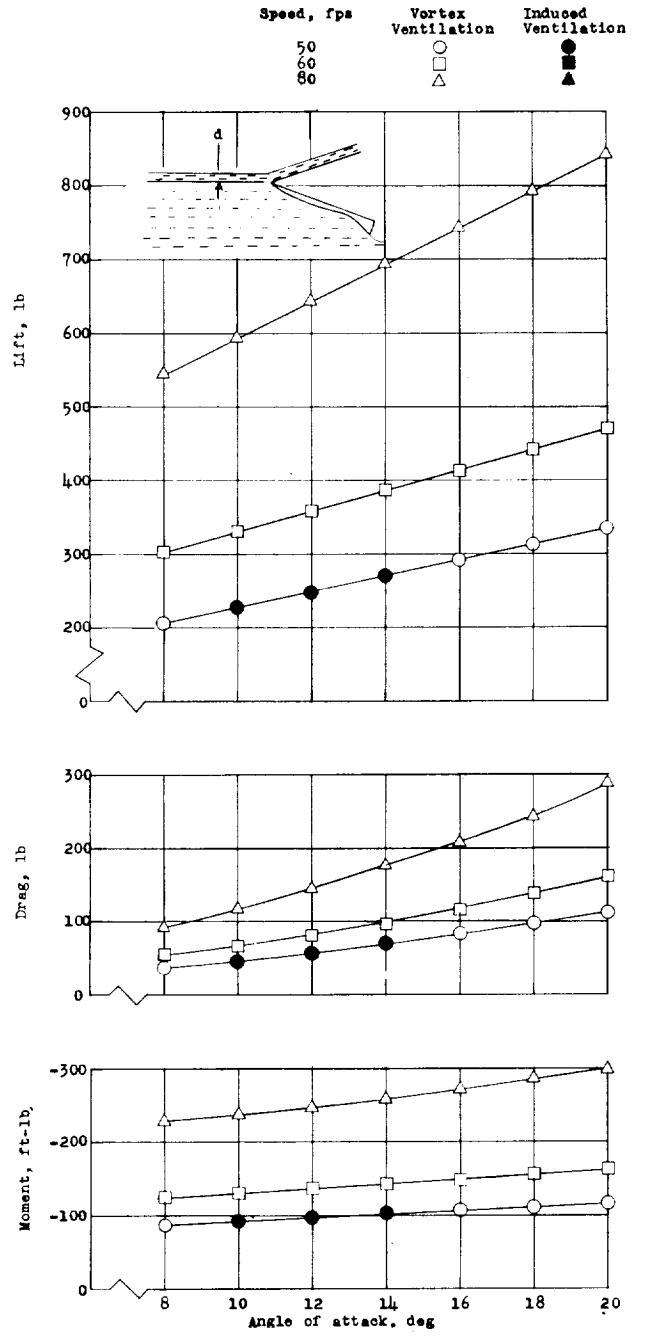

(a) d = 0 inch.

Figure 7.- Zero-cavitation-number characteristics of the aspect-ratio-1 hydrofoil.

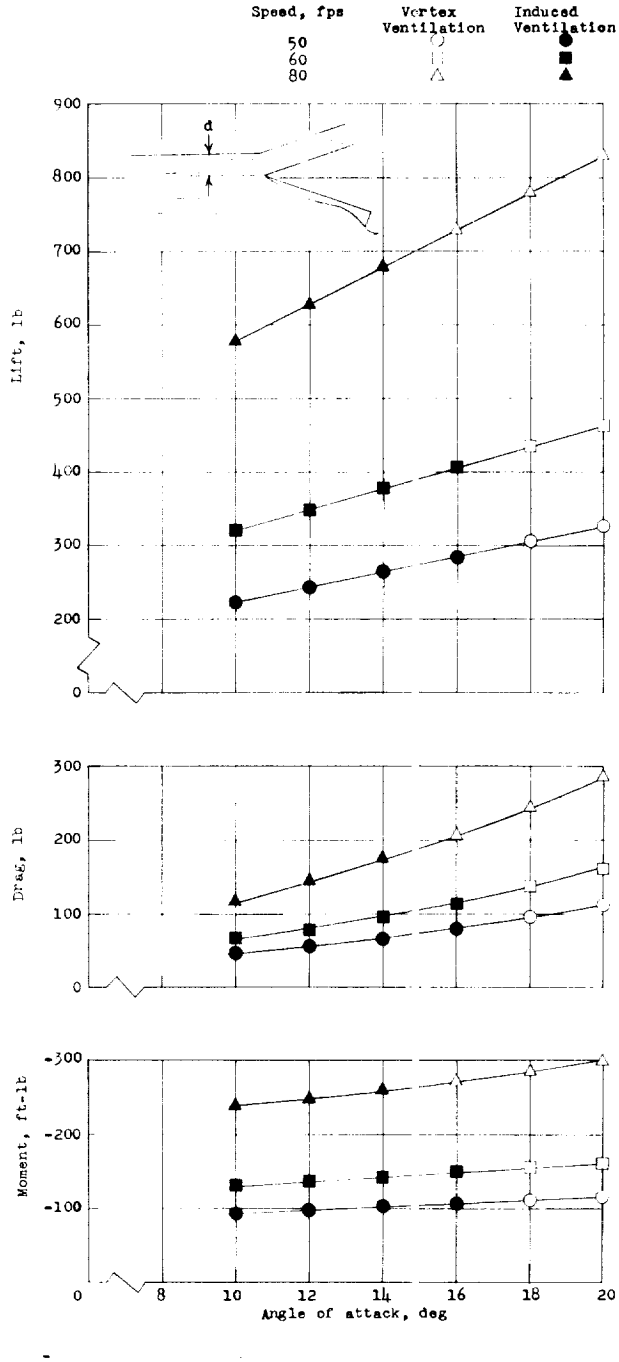

(b) d = 0.5 inch.

Figure 7.- Continued.

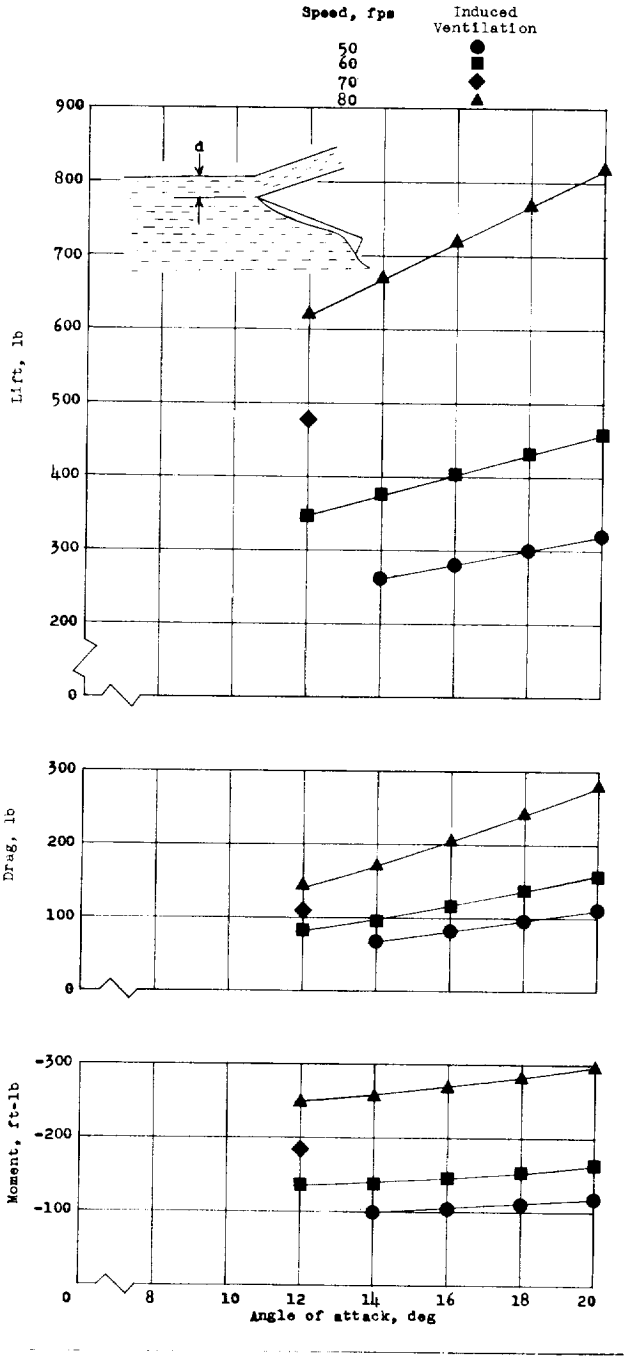

(c) d = 1.0 inch.

Figure 7.- Continued.

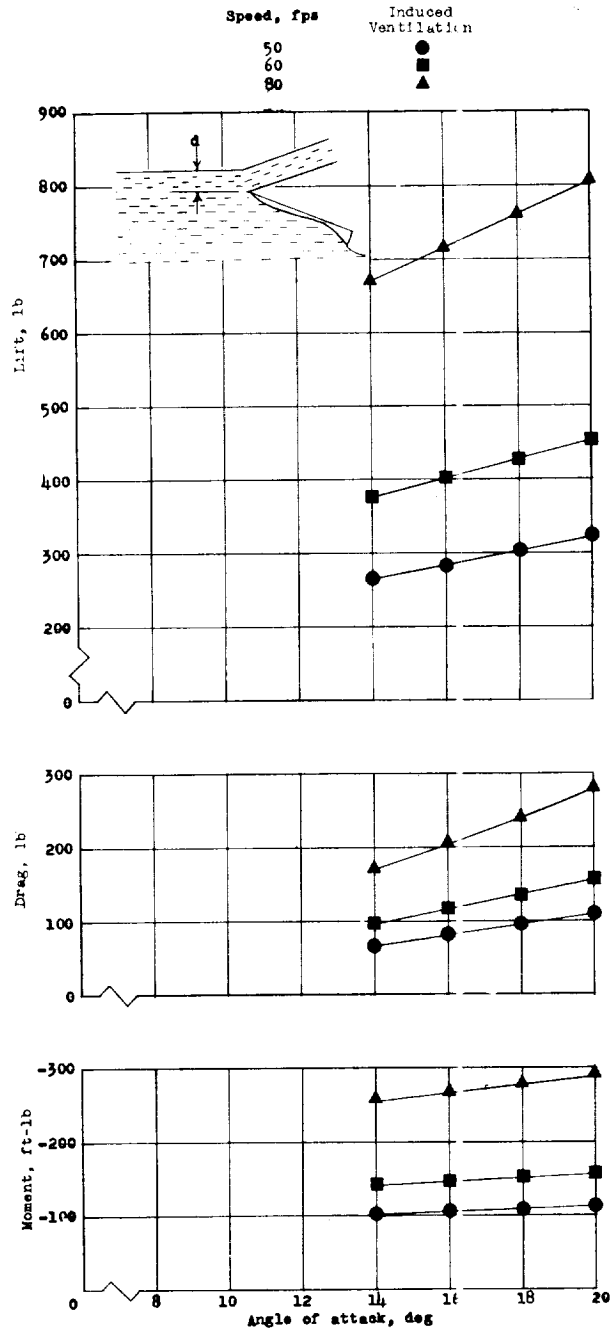

(d) d = 2.0 inches.

Figure 7.- Continued.

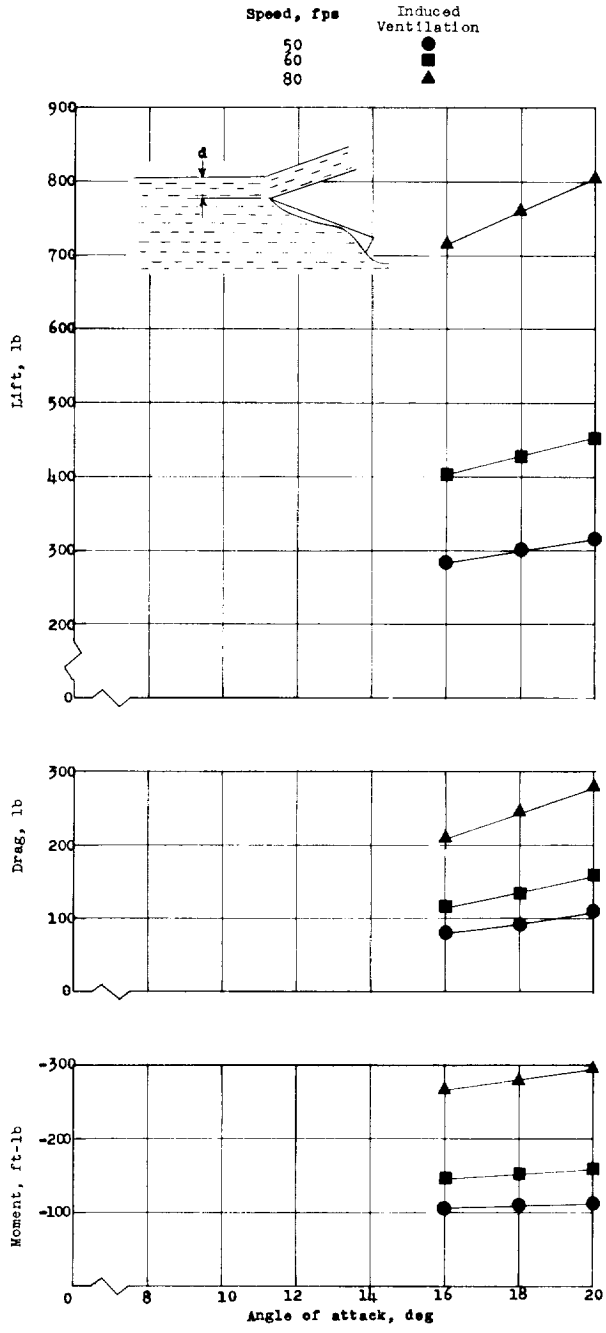

(e) d = 4.0 inches.

Figure 7.- Continued.

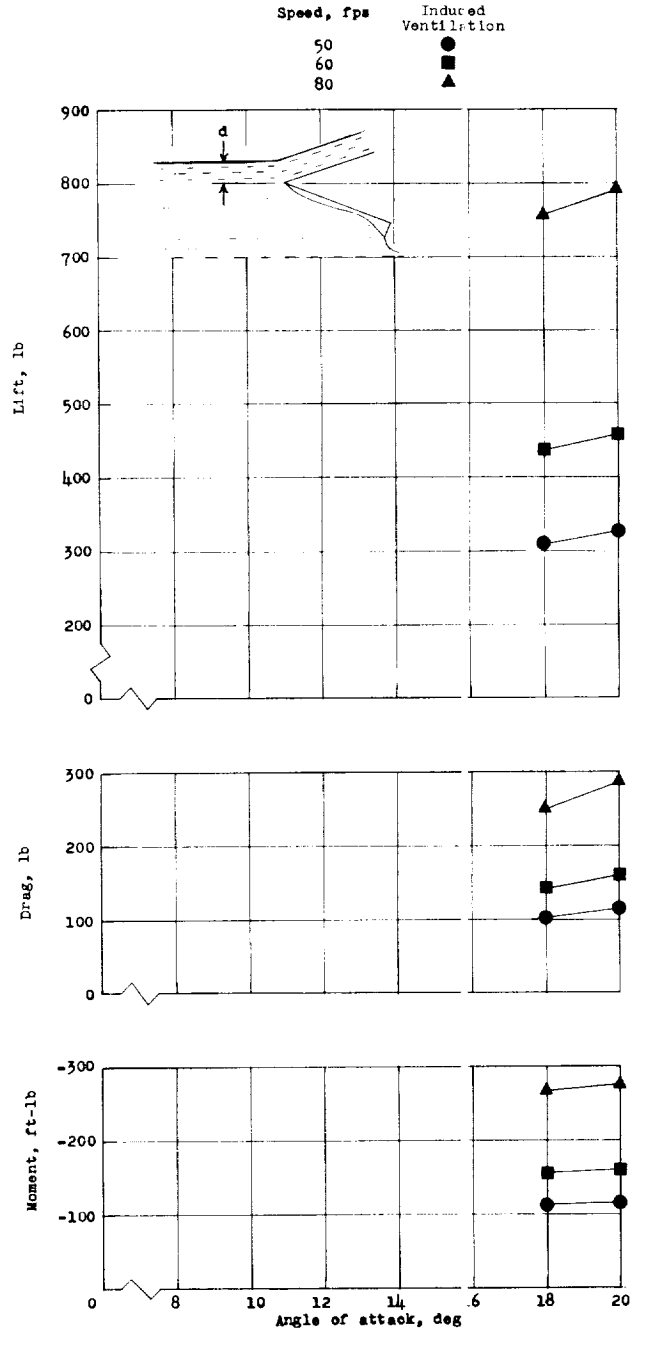

(f) d = 6.0 inches.

Figure 7.- Concluded.

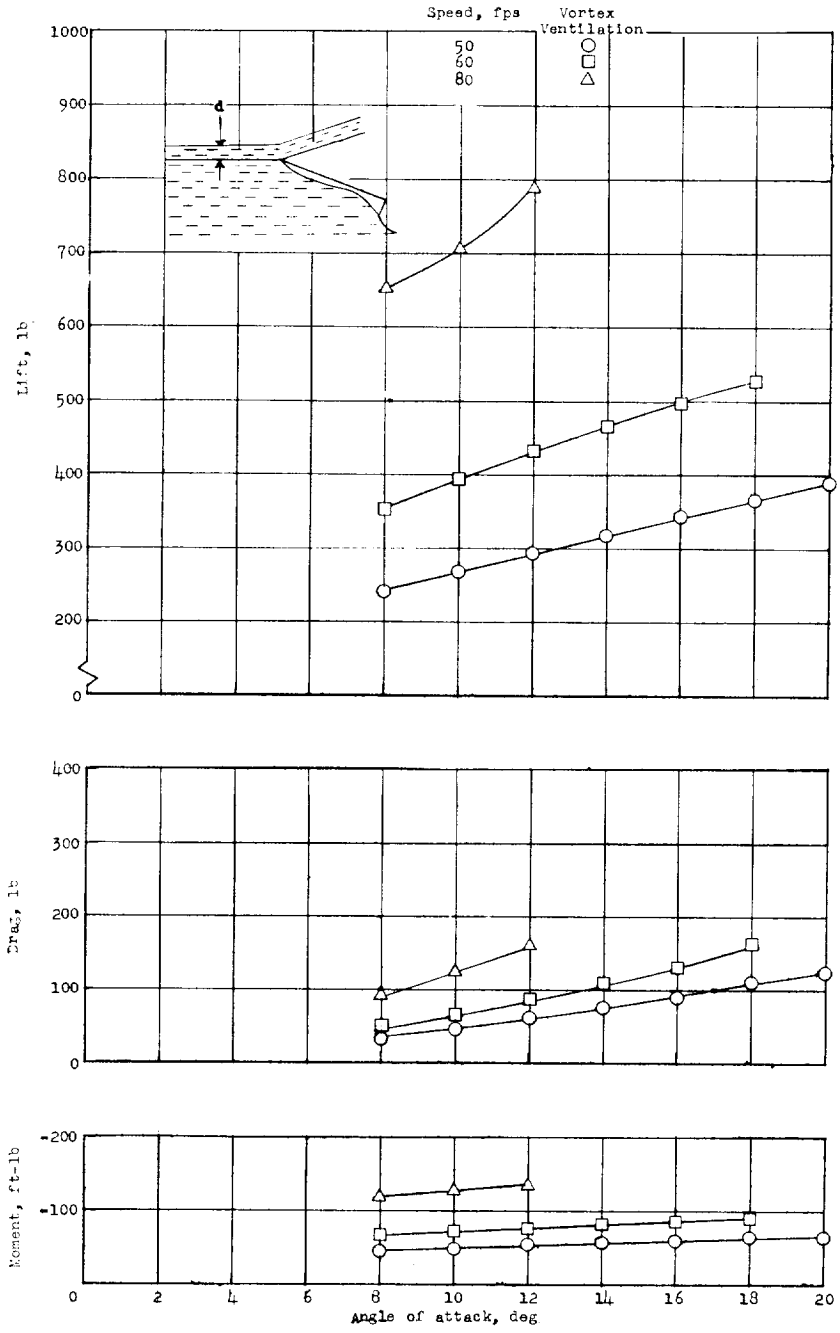

(a) d = 0 inch.

Figure 8.- Zero-cavitation-number characteristics of the aspect-ratio-3 hydrofoil.

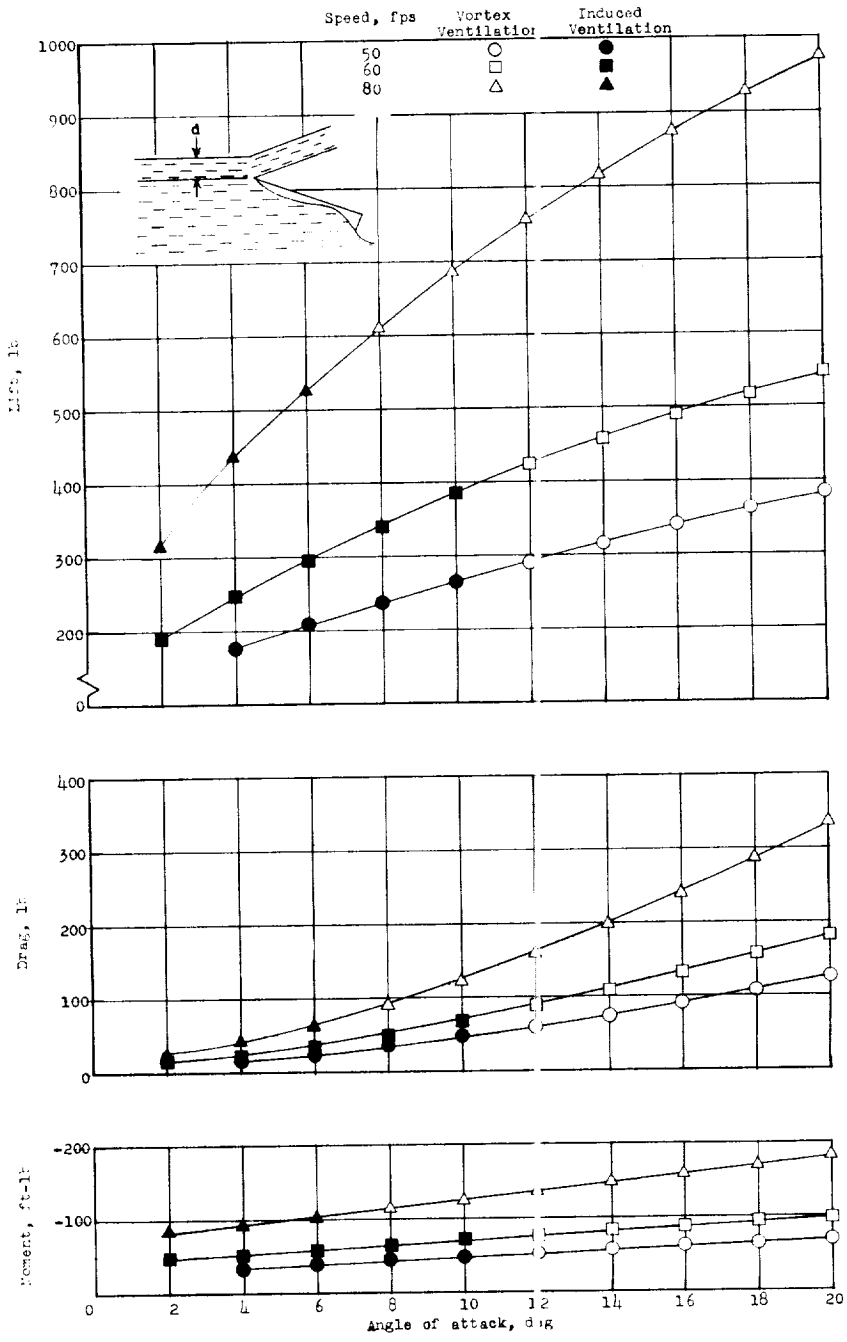

(b) d = 0.29 inch.

Figure 8.- Continued.

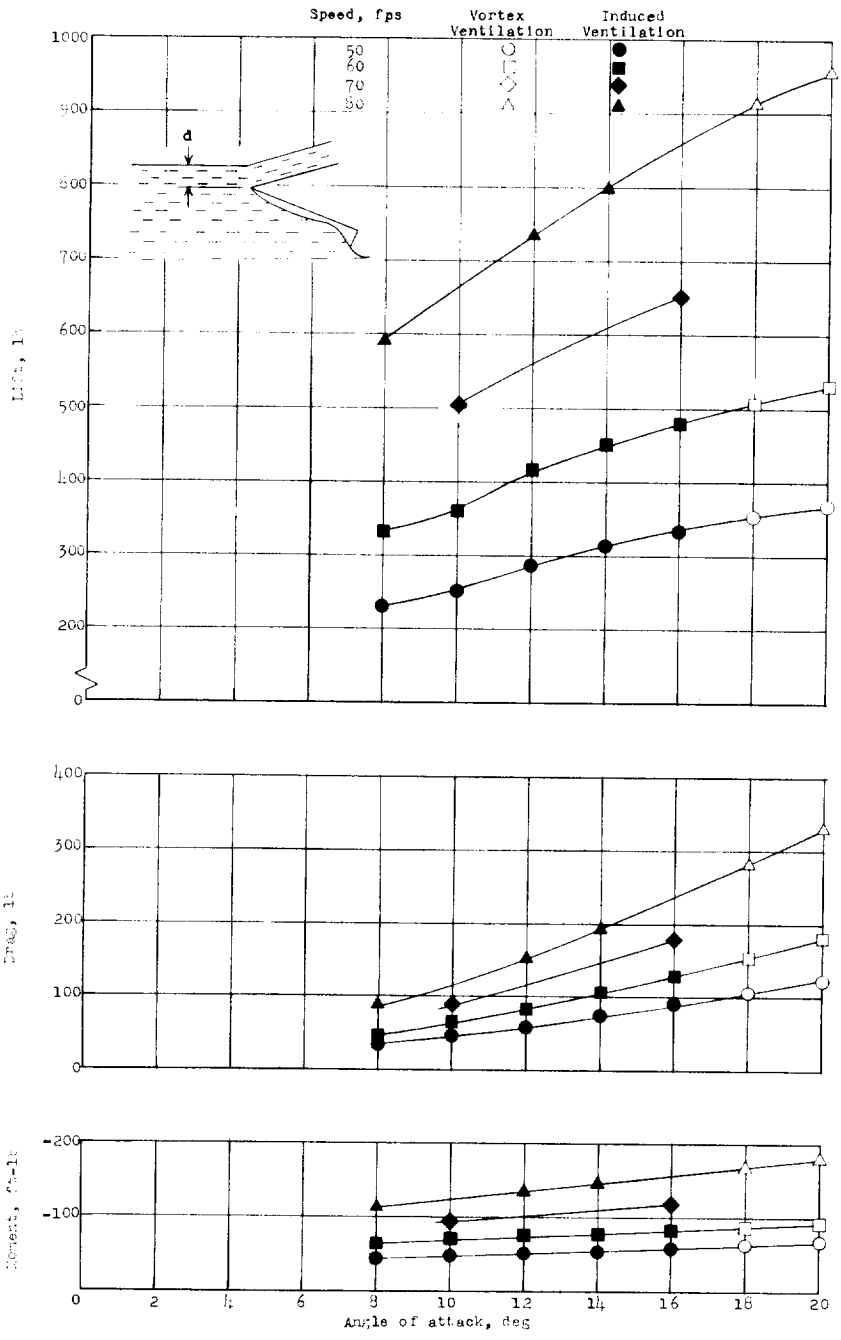

(c) d = 0.58 inch.

Figure 8.- Continued.

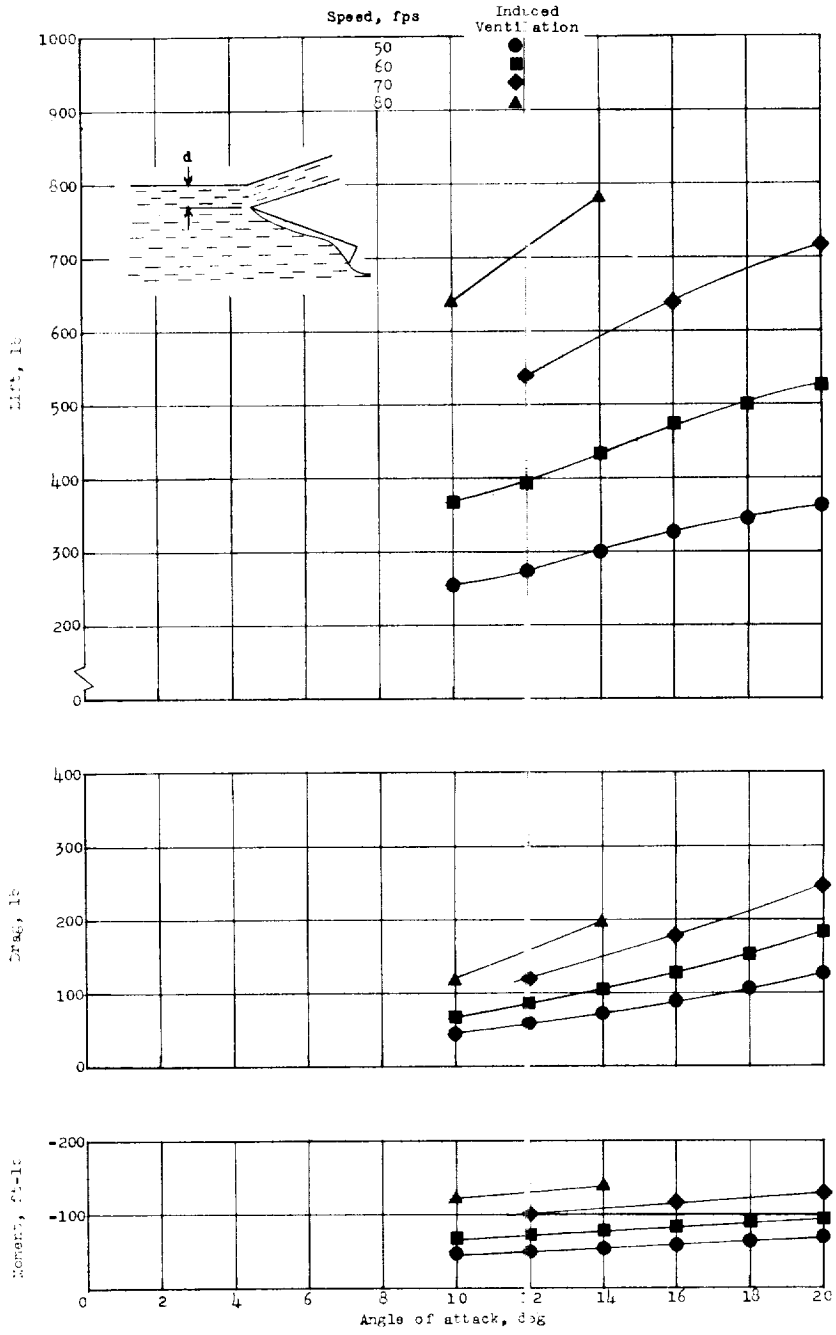

(d) d = 1.15 inches.

Figure 8.- Continued.

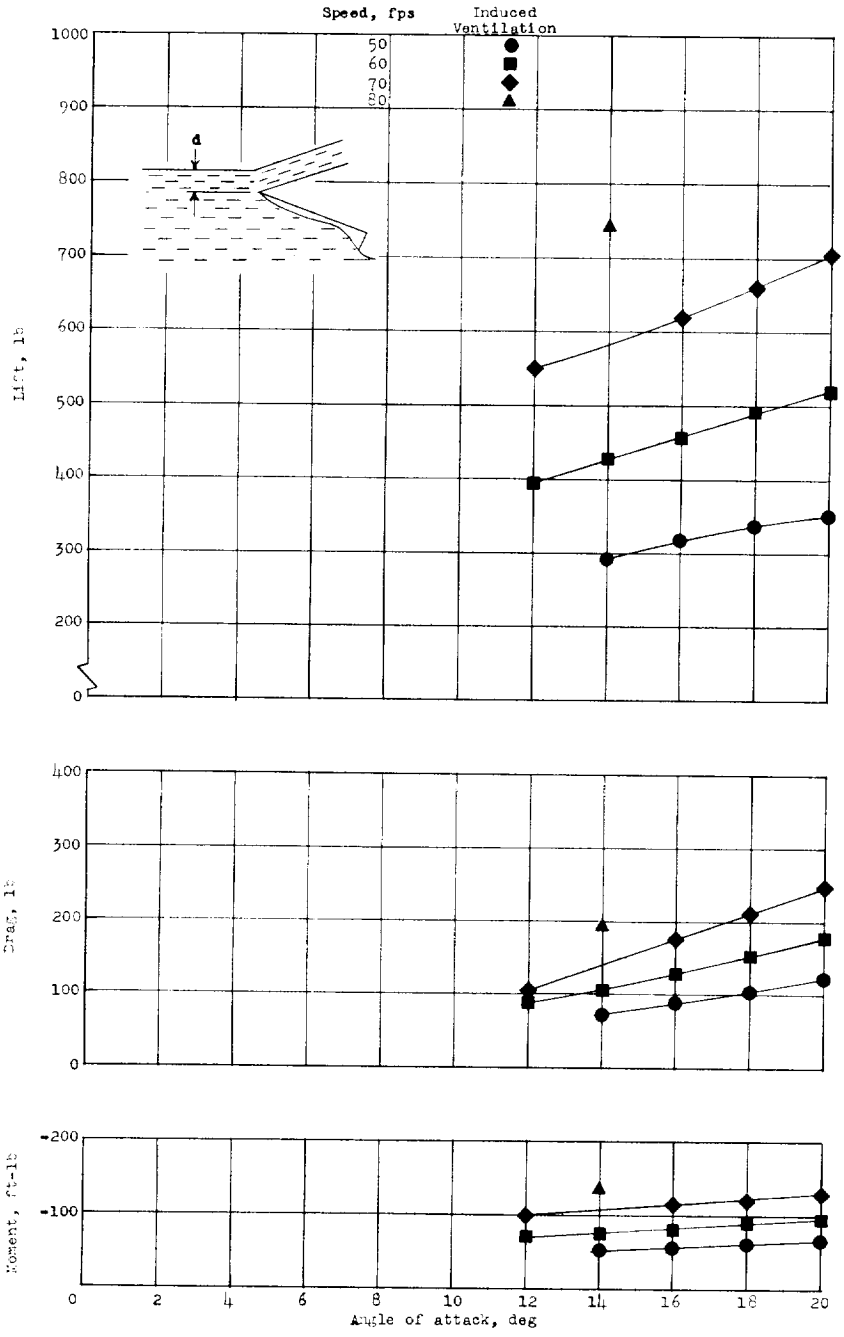

(e) d = 2.31 inches.

Figure 8.- Continued.

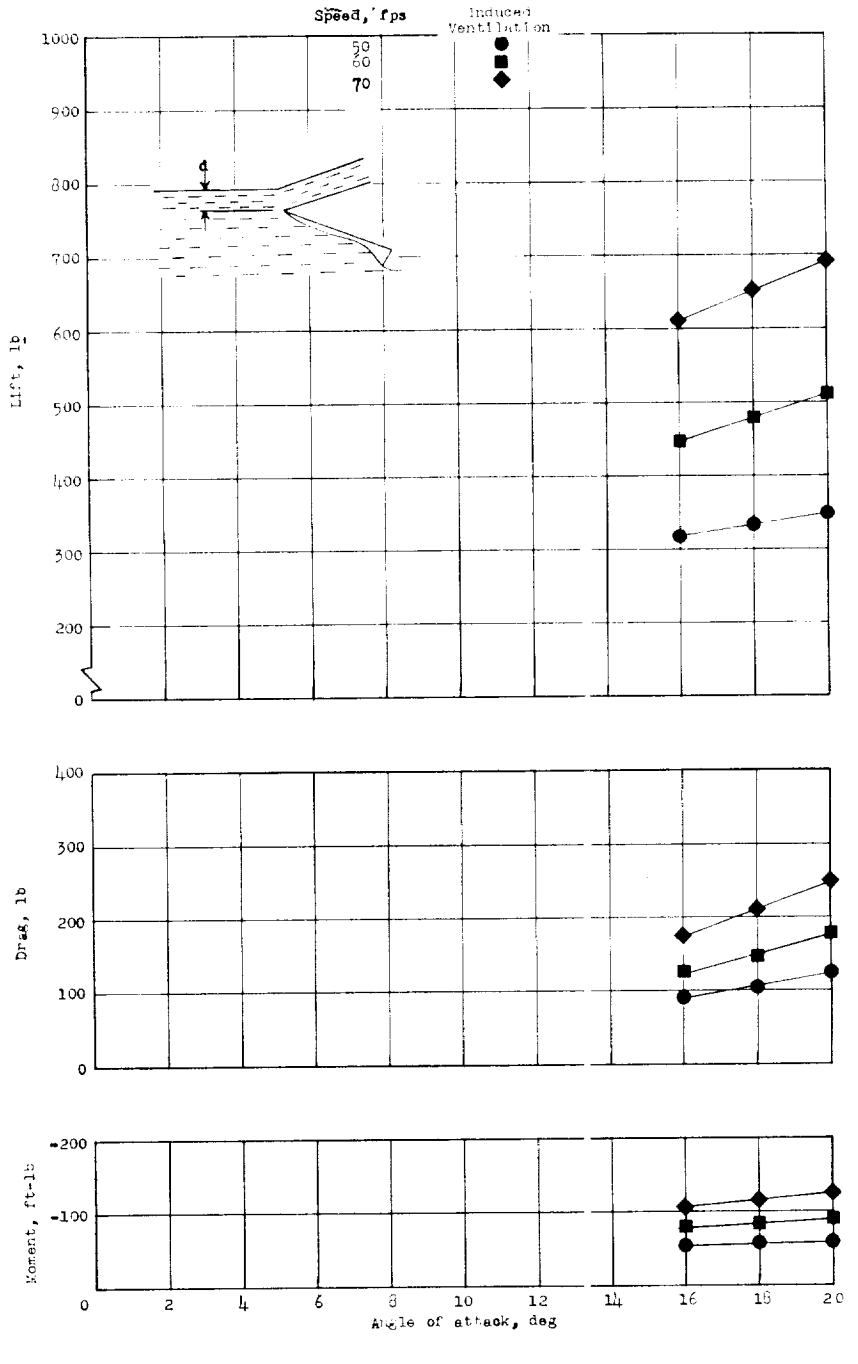

(f) d = 3.47 inches.

Figure 8.- Concluded.

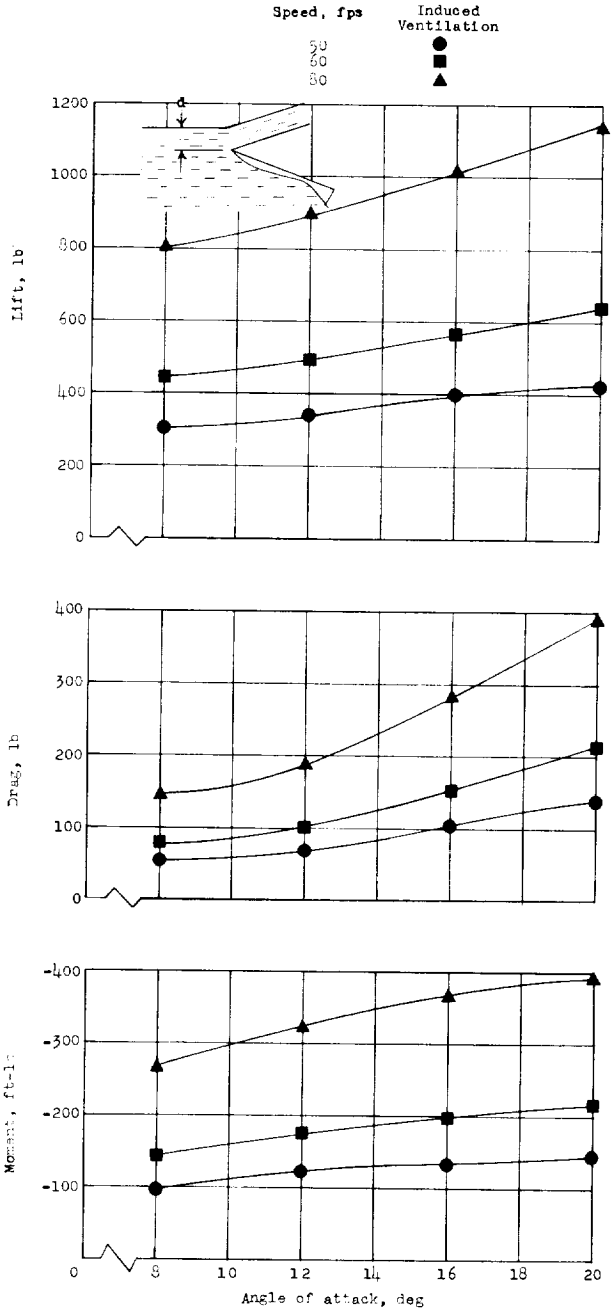

(a) Large end plates.

Figure 9.- Zero-cavitation-number characteristics of the aspect-ratio-1 hydrofoil with end plates. d = 0.5 inch.

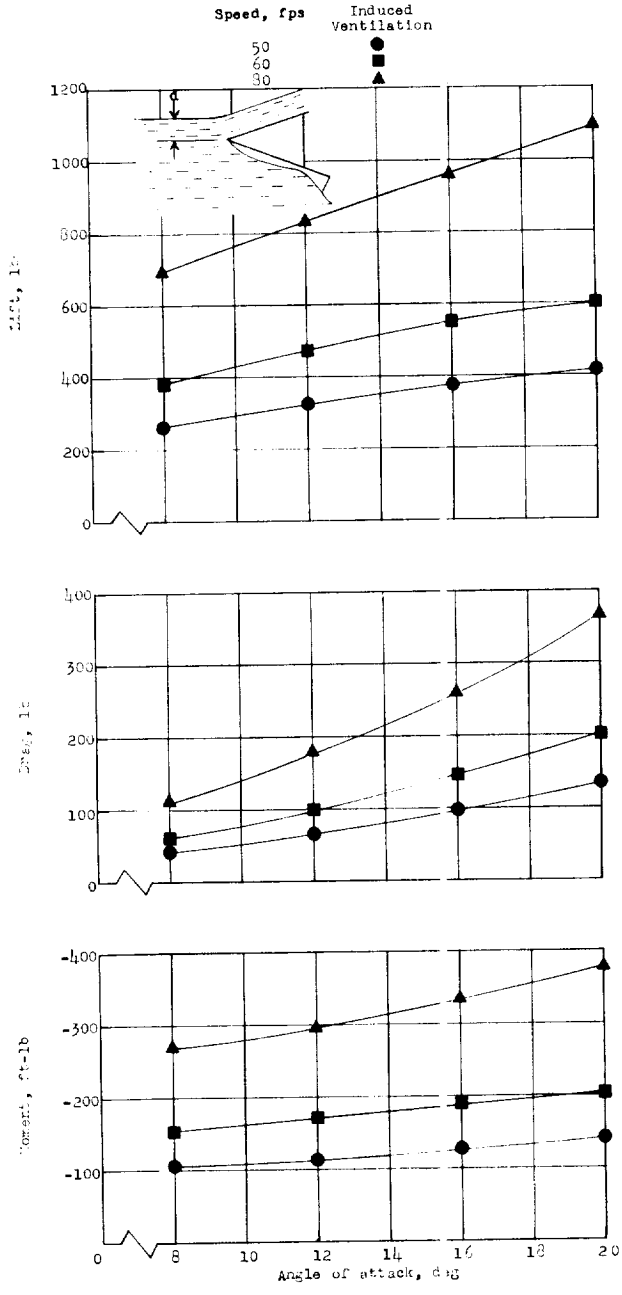

(b) Small end plates.

Figure 9.- Concluded.

(a) Aspect-ratio-1 hydrofoil.

(b) Aspect-ratio-3 hydrofoil.

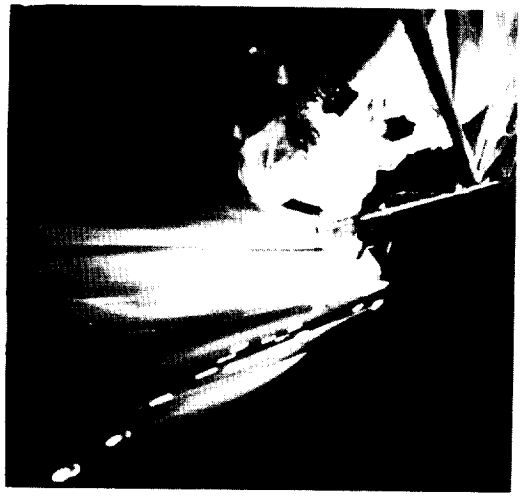

(c) Aspect-ratio-1 hydrofoil with large end plates.

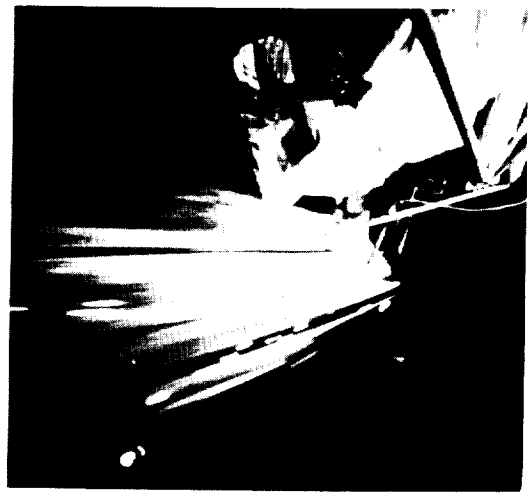

(d) Aspect-ratio-1 hydrofoil with small end plates.

L-59-205

Figure 10.- Ventilated flow about all model configurations. $\frac{d}{c} = 0.071$; $\alpha = 20^{\circ}$; V = 50 fps.

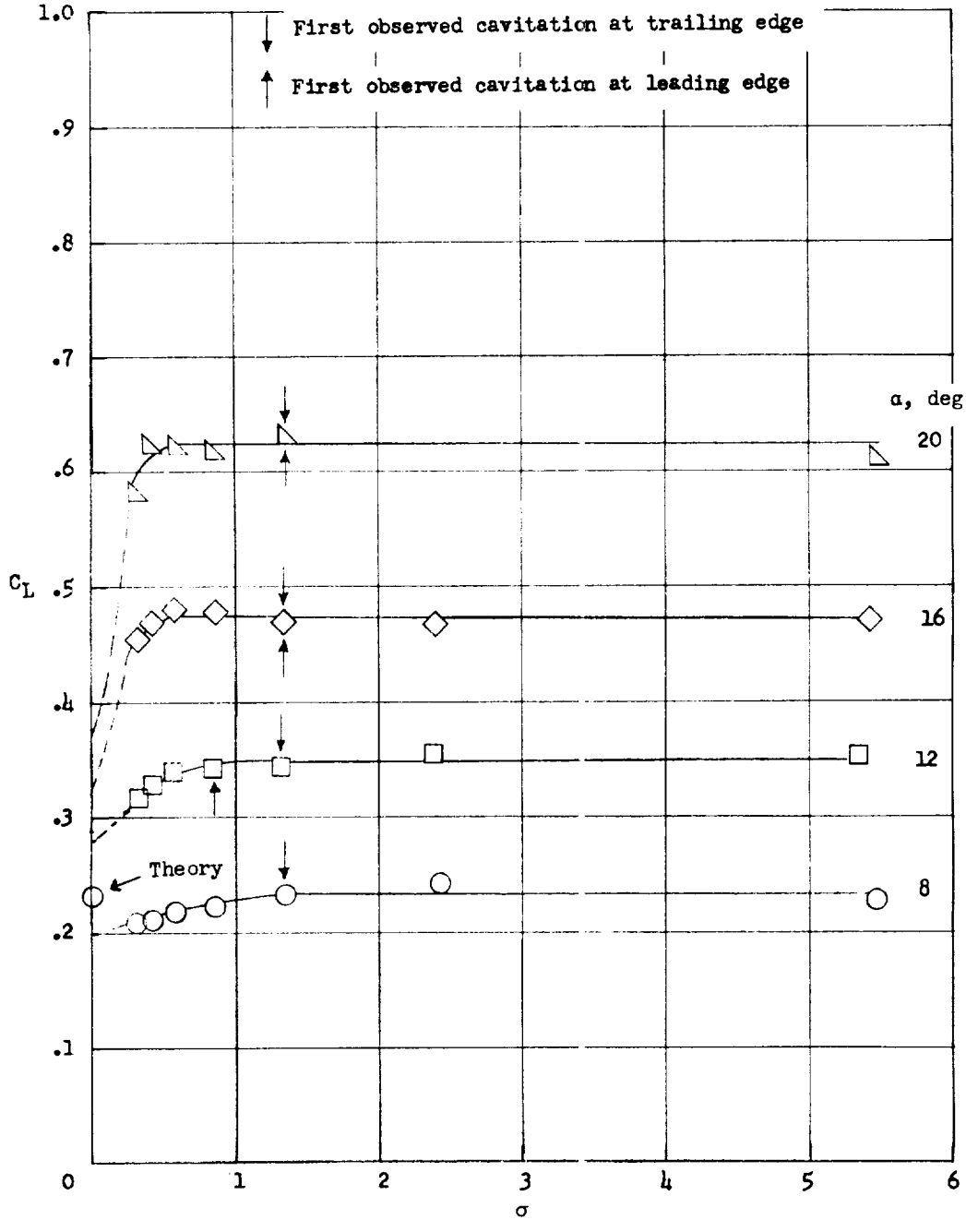

(a) Lift coefficient.

Figure 11.- Effect of cavitation number on the lift and drag characteristics of the aspect-ratio-1 hydrofoil. d = 6.0 inches.

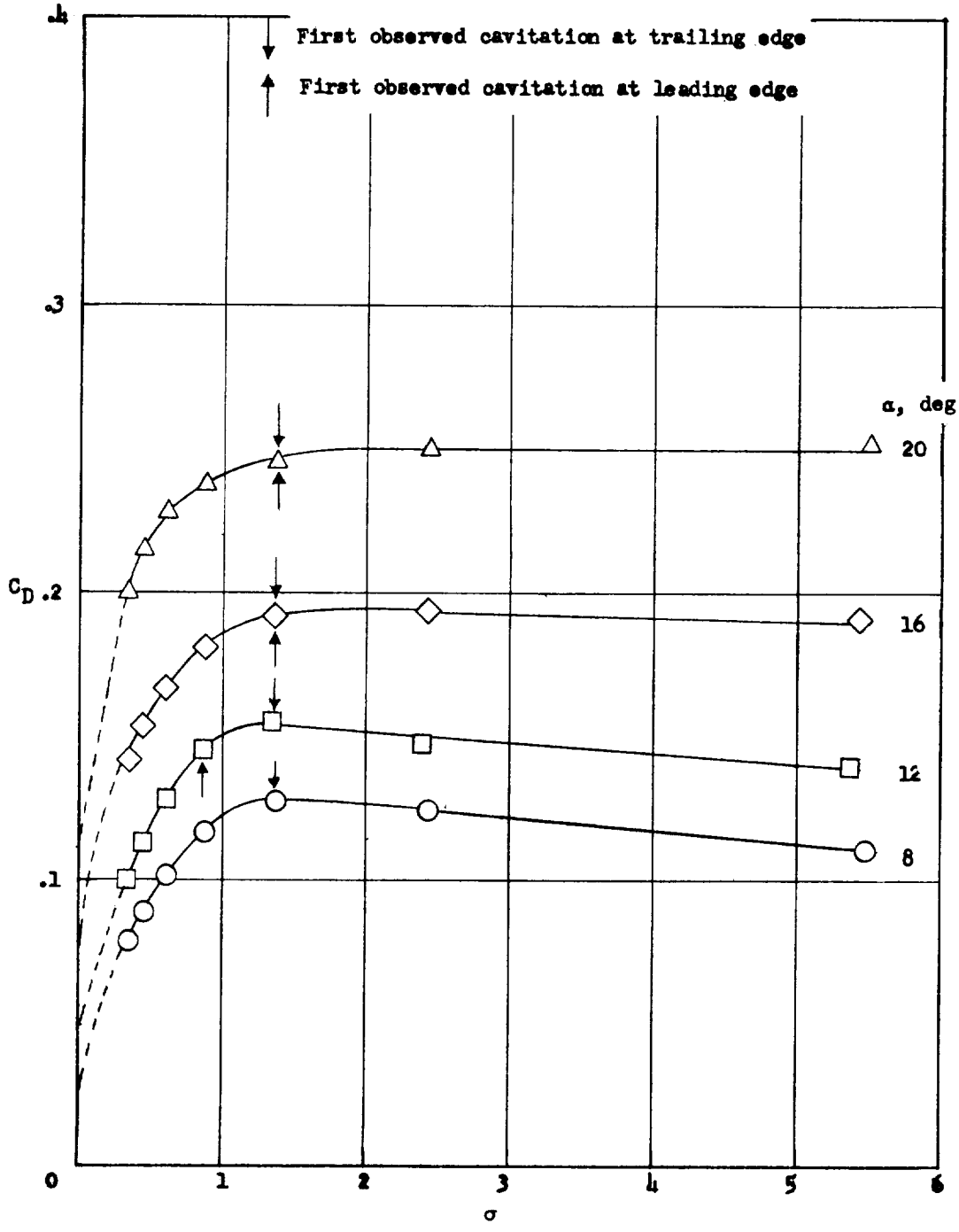

(b) Drag coefficient.

Figure 11.- Concluded.

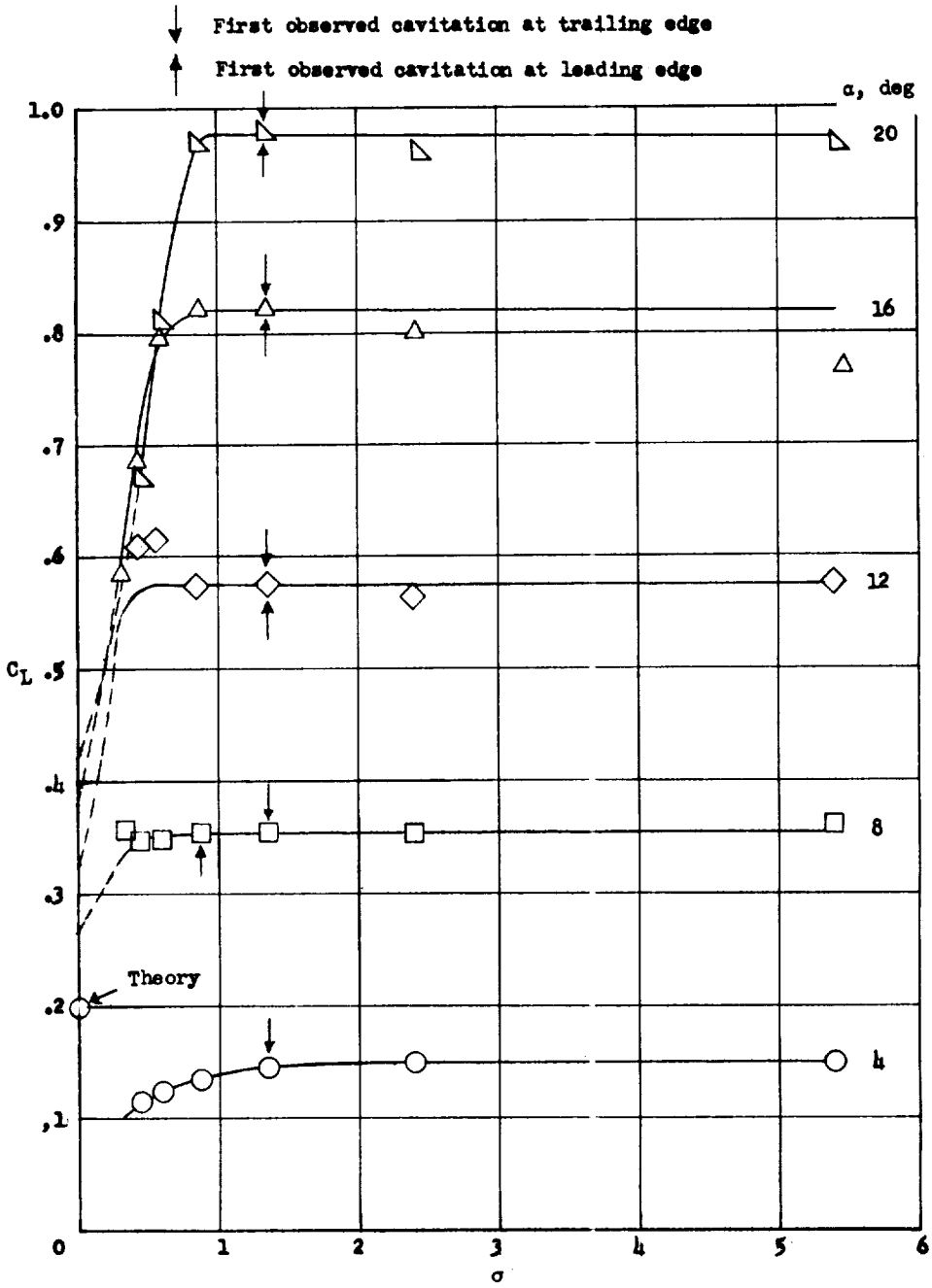

(a) Lift coefficient.

Figure 12.- Effect of cavitation number on the lift and drag characteristics of the aspect-ratio-3 hydrofoil. d = 3.47 inches.

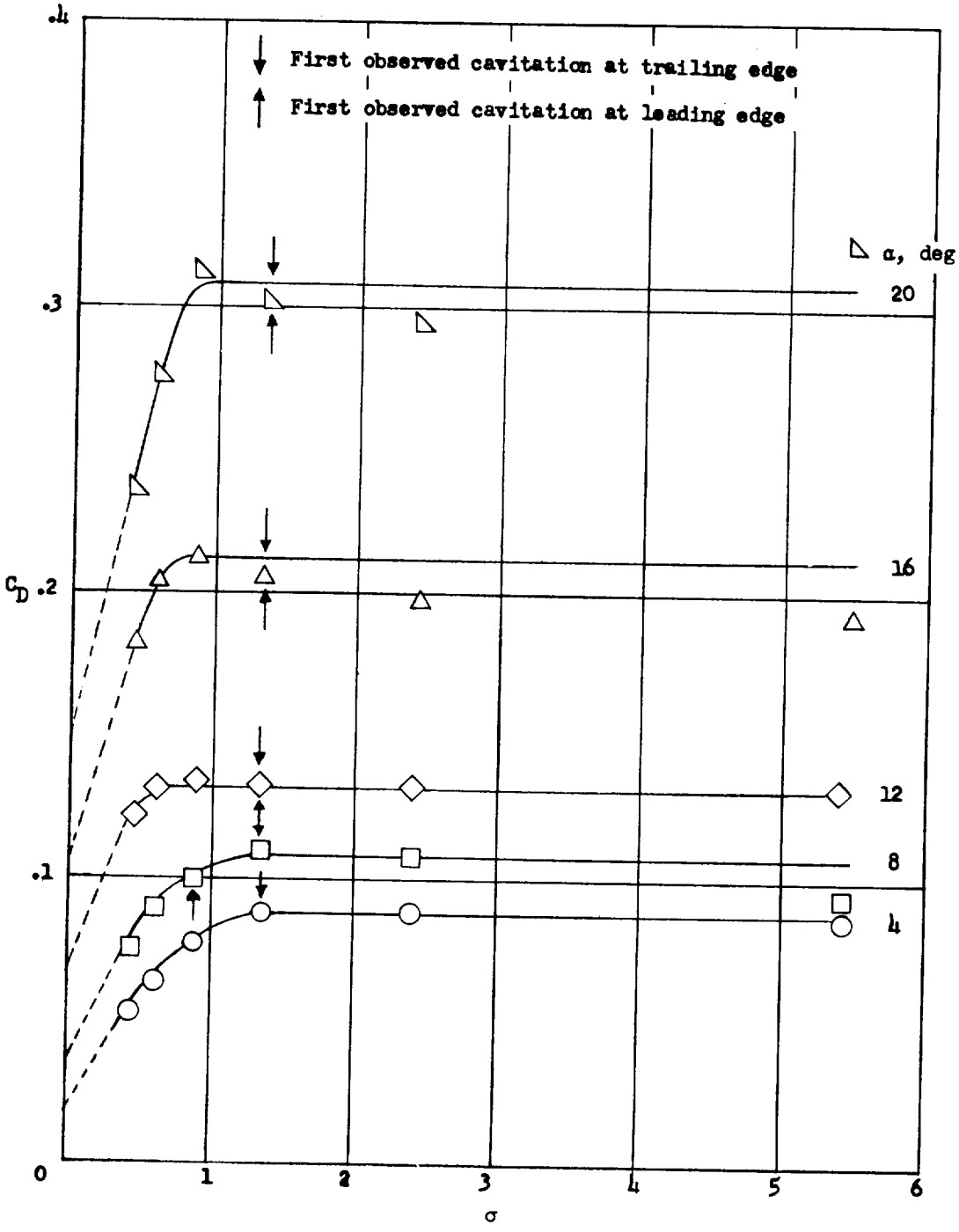

(b) Drag coefficient.

Figure 12.- Concluded.

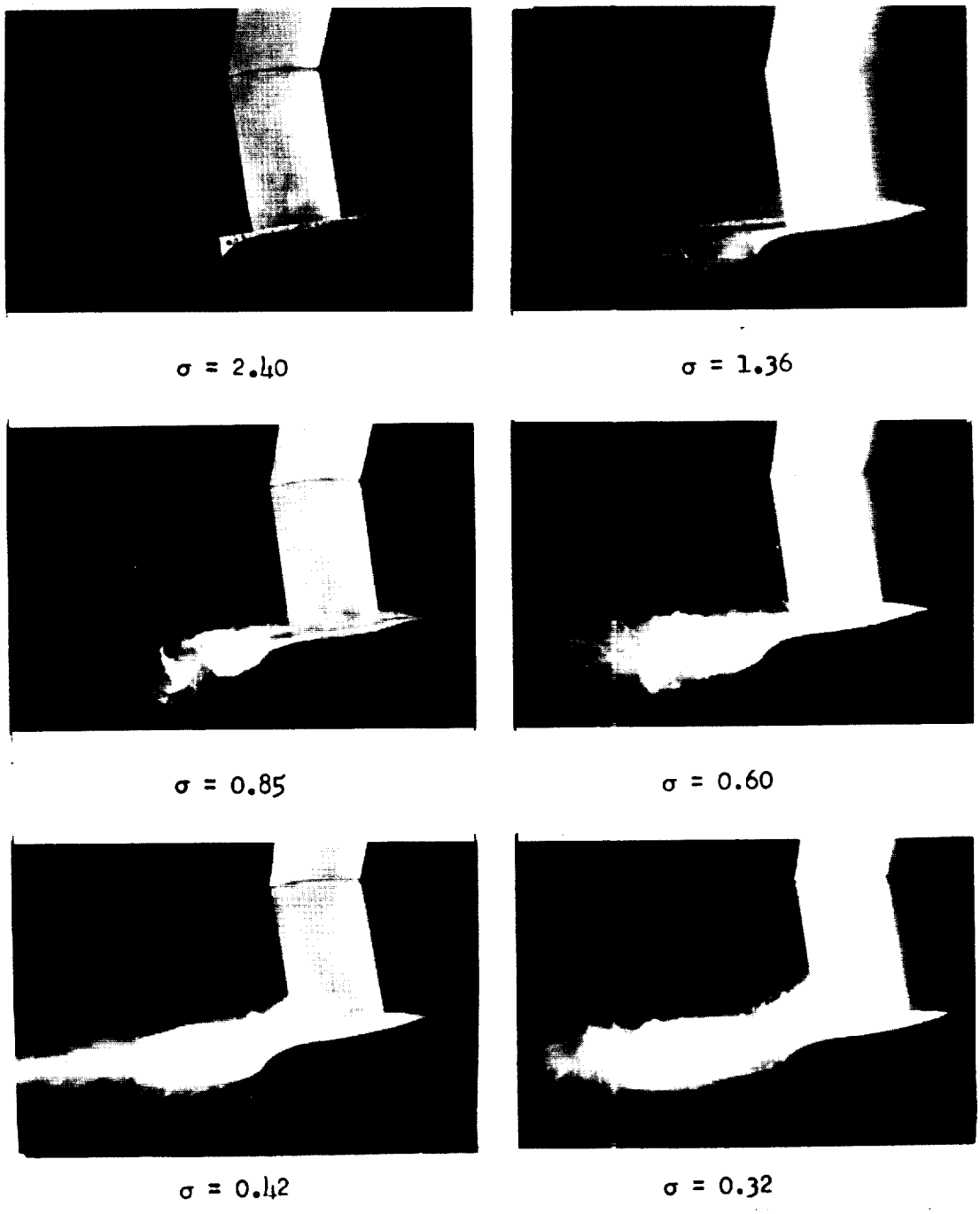

(a) Aspect-ratio-1 hydrofoil. (d = 6.0 inches.) L-59-206

Figure 13.- Photographs of flow at finite cavitation numbers. $\alpha = 20^{\circ}$.

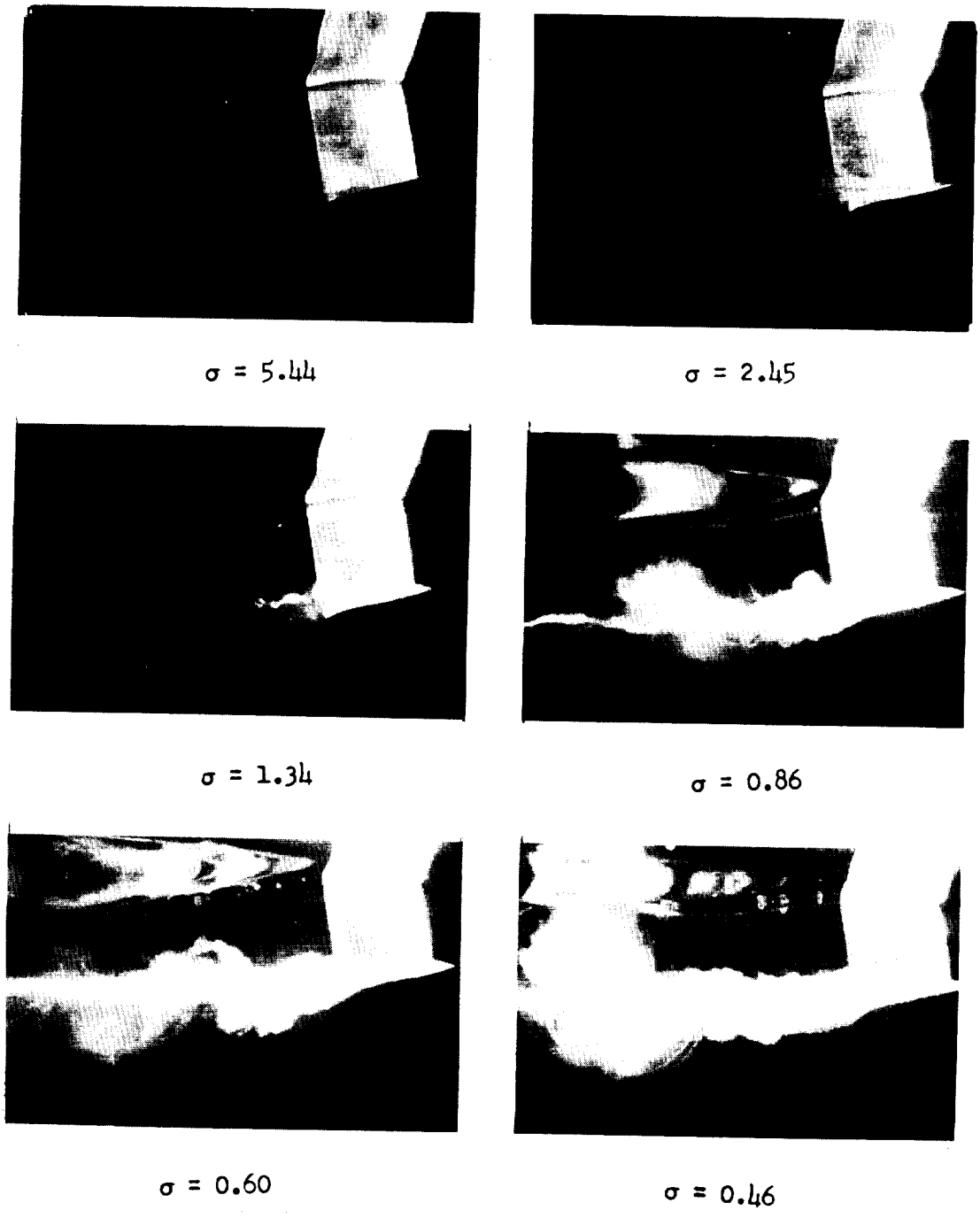

(b) Aspect-ratio-3 hydrofoil. (d = 3.47 inches.) L-59-207

Figure 13.- Concluded.

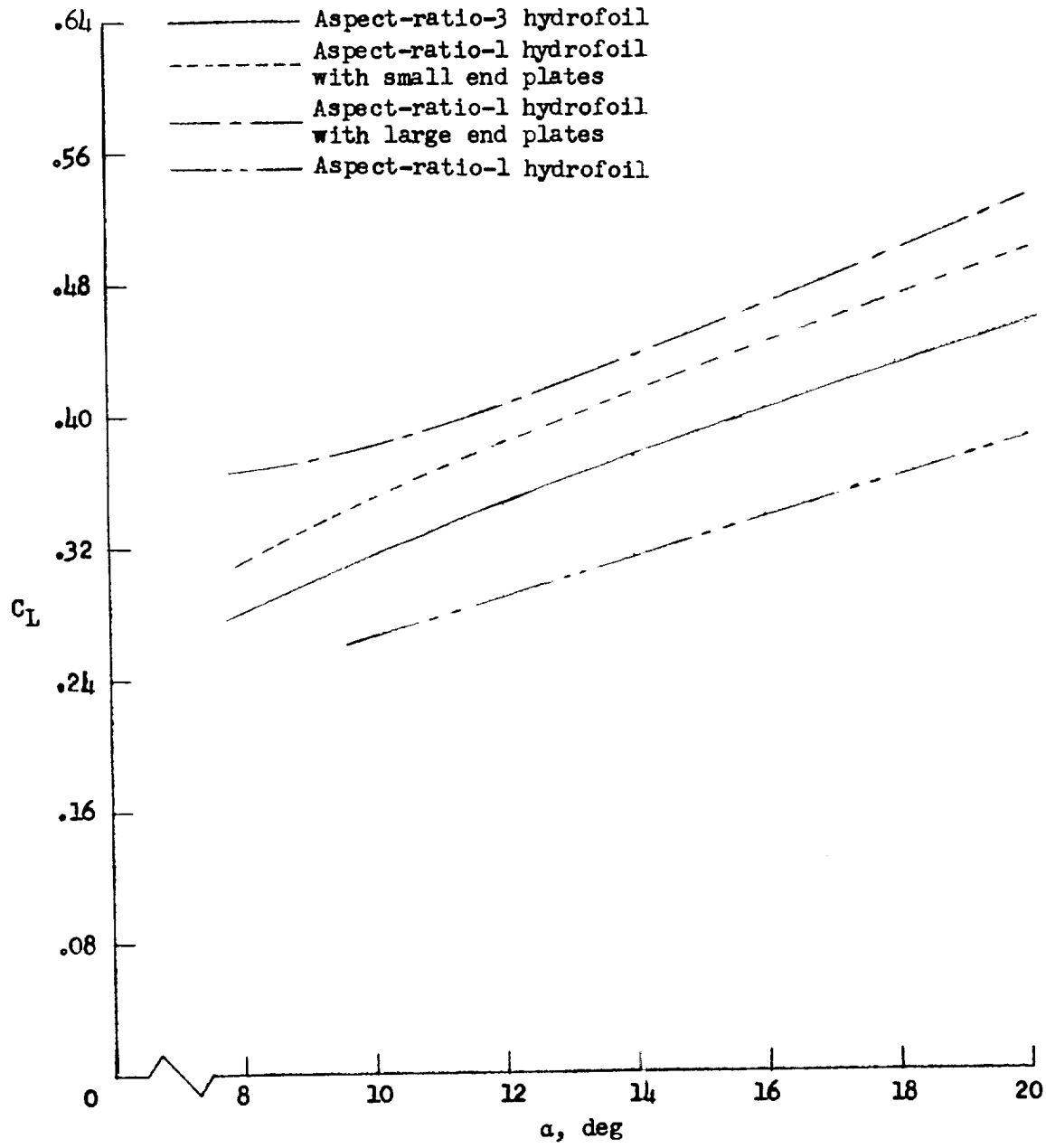

(a) Lift coefficient.

Figure 14.- Comparison of lift coefficients, lift-drag ratios, and centers of pressure for all model configurations. d/c = 0.071; σ = 0.

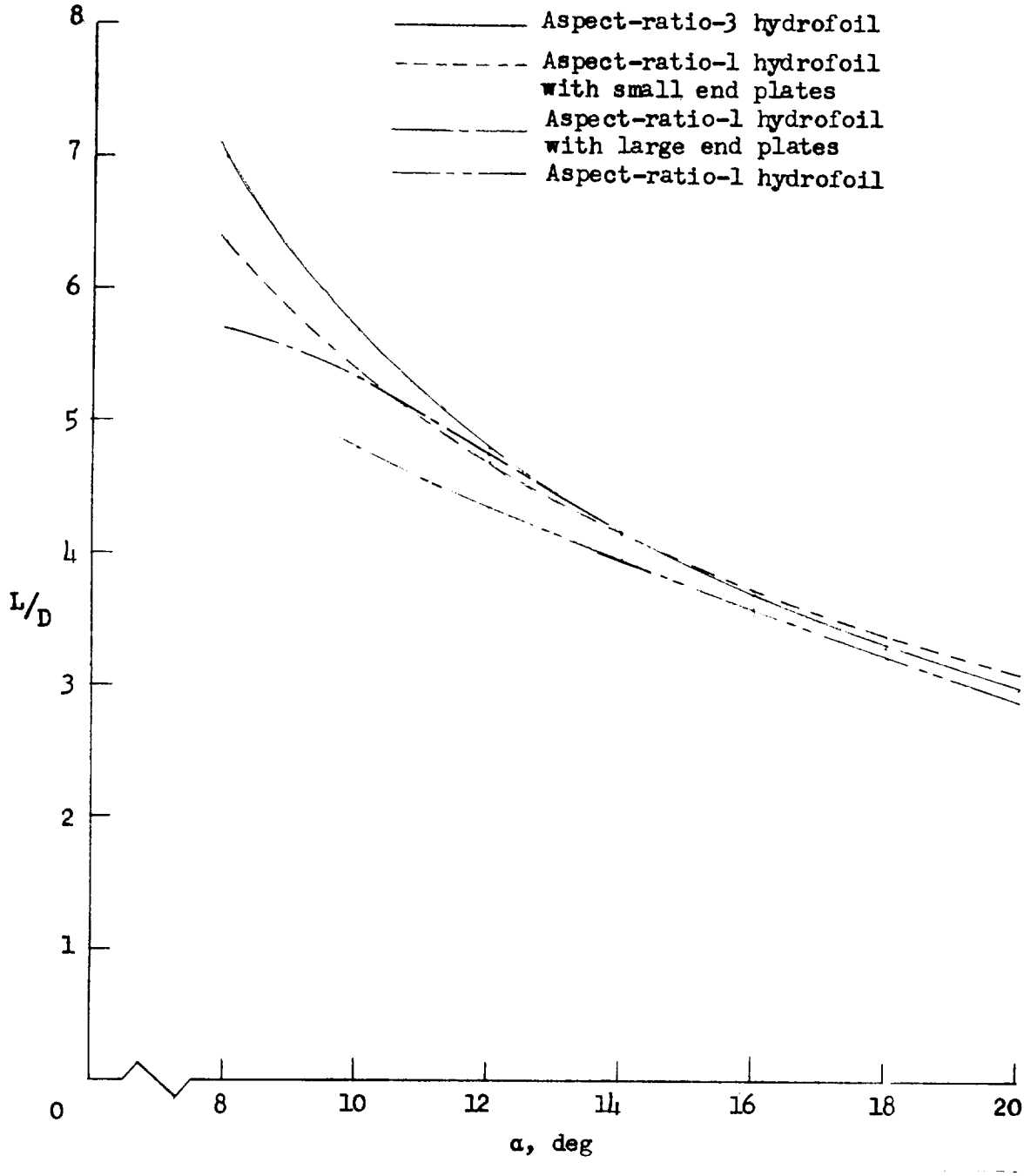

(b) Lift-drag ratios.

Figure 14.- Continued.

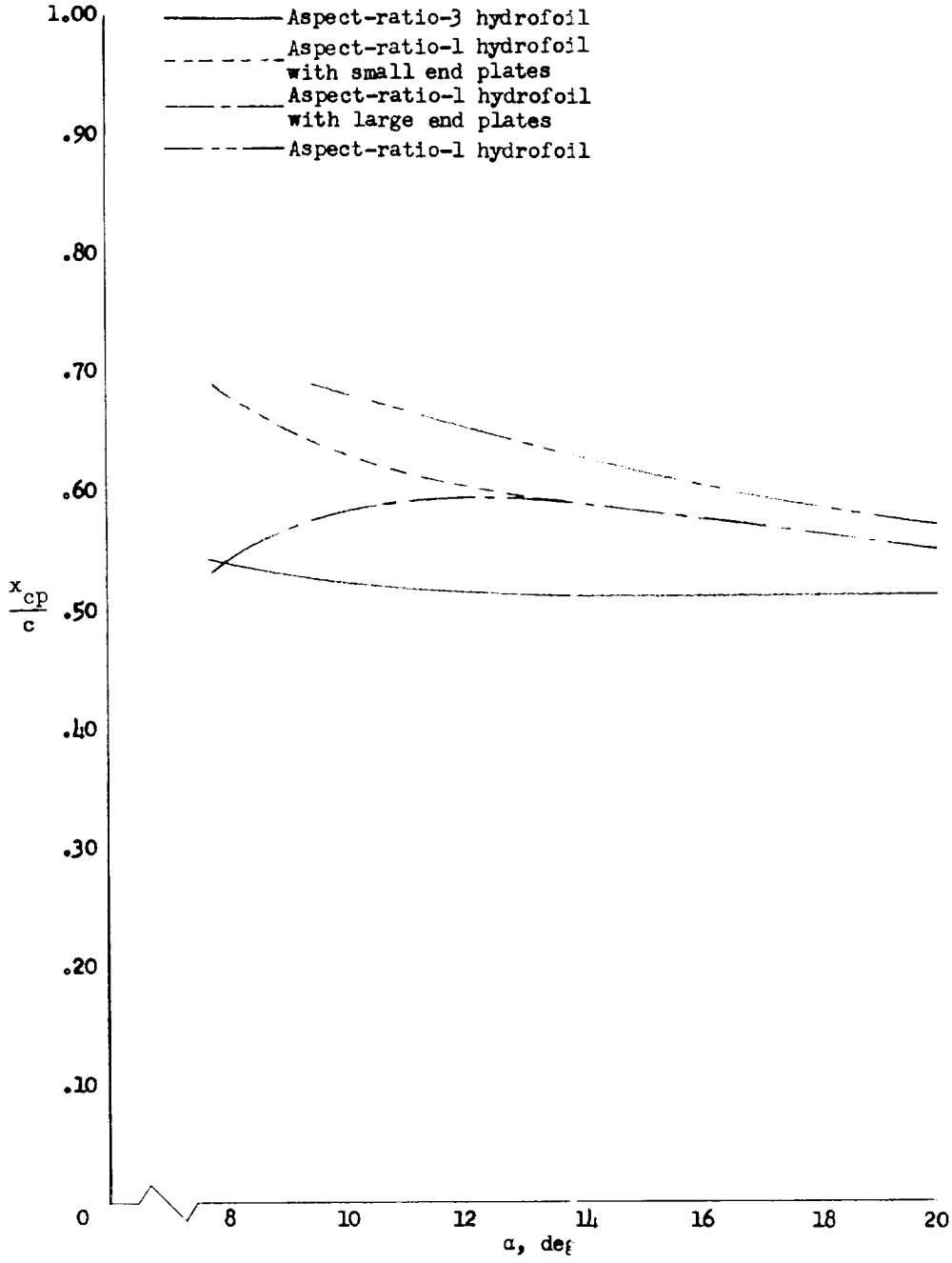

(c) Ratio of distance of center of pressure rearward of leading edge to chord.

Figure 14.- Concluded.

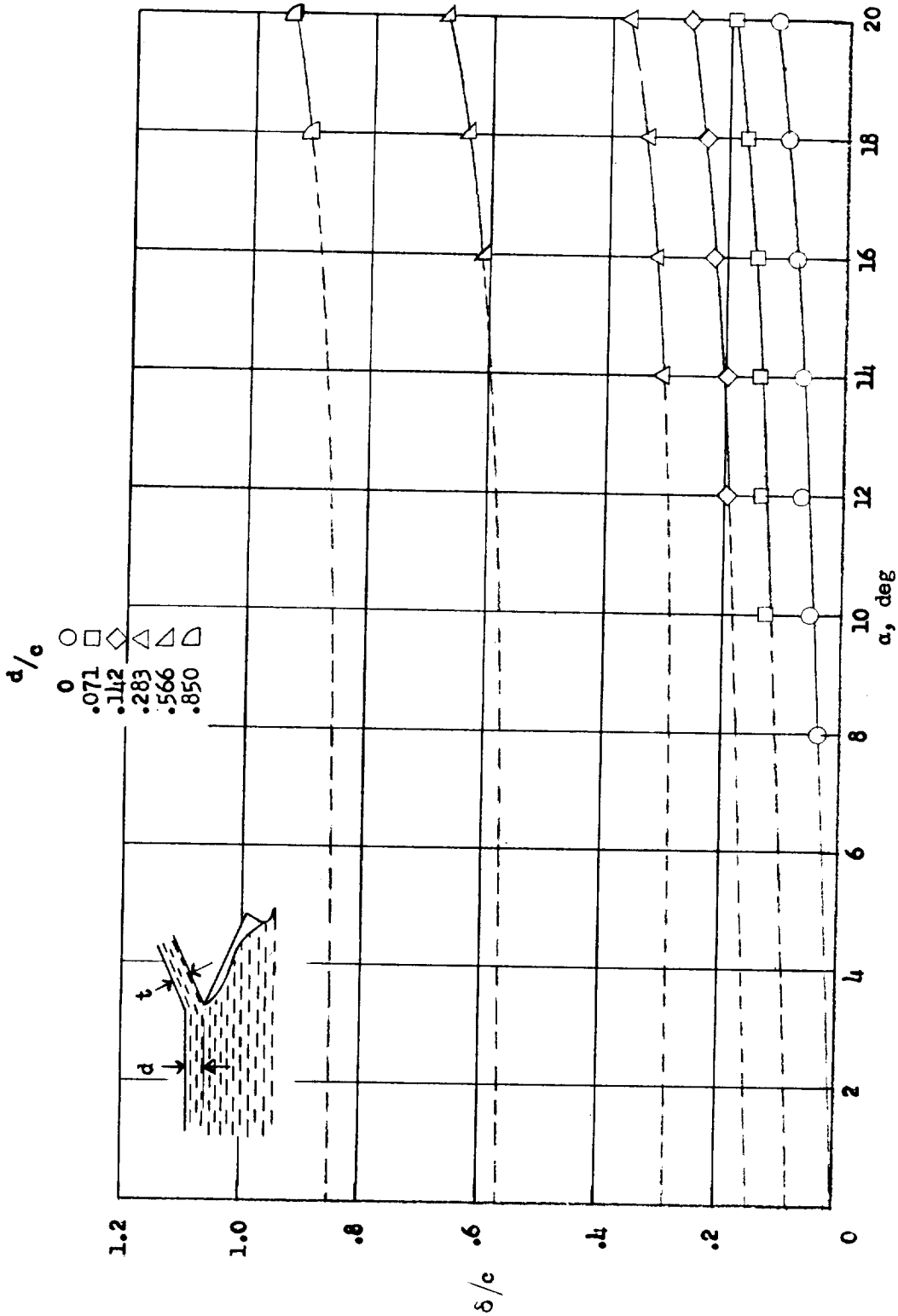

(a) Aspect-ratio-1 hydrofoil.

Figure 15.- Ratio of spray thickness to chord.

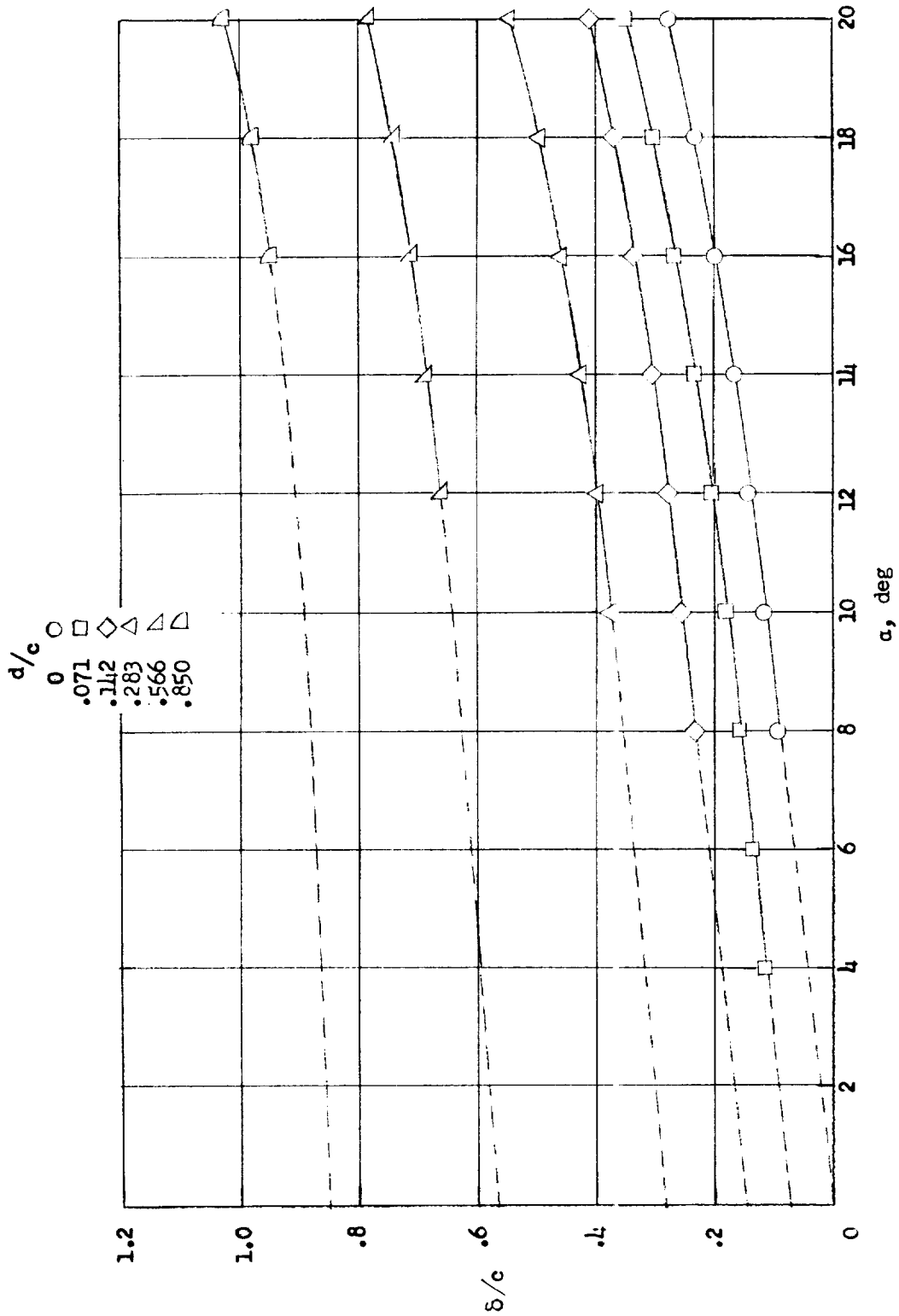

(b) Aspect-ratio-3 hydrofoil.

Figure 15.- Concluded.

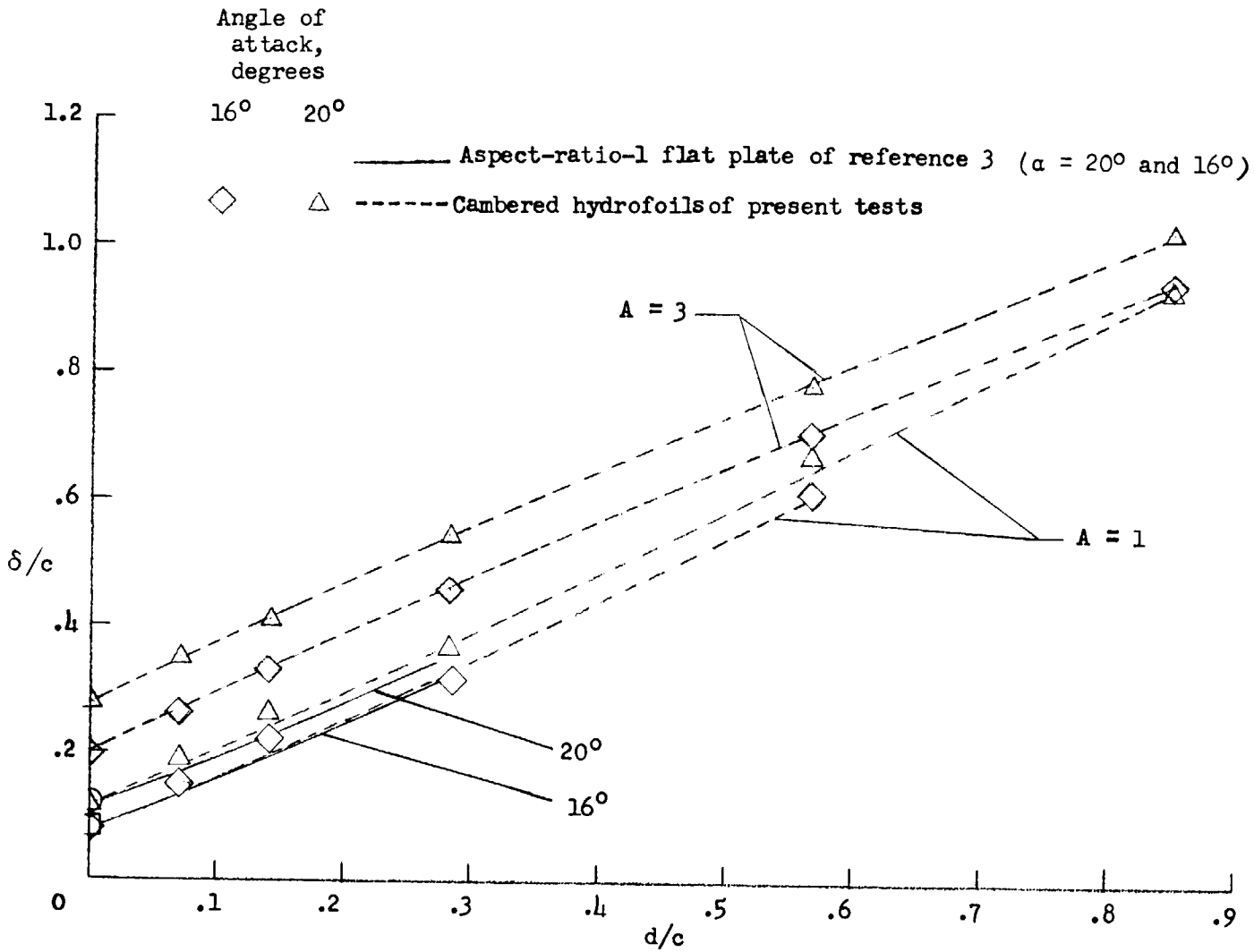

Figure 16.- Comparison of spray thickness for cambered hydrofoils of present test with that of aspect-ratio-1 flat plate of reference 3.

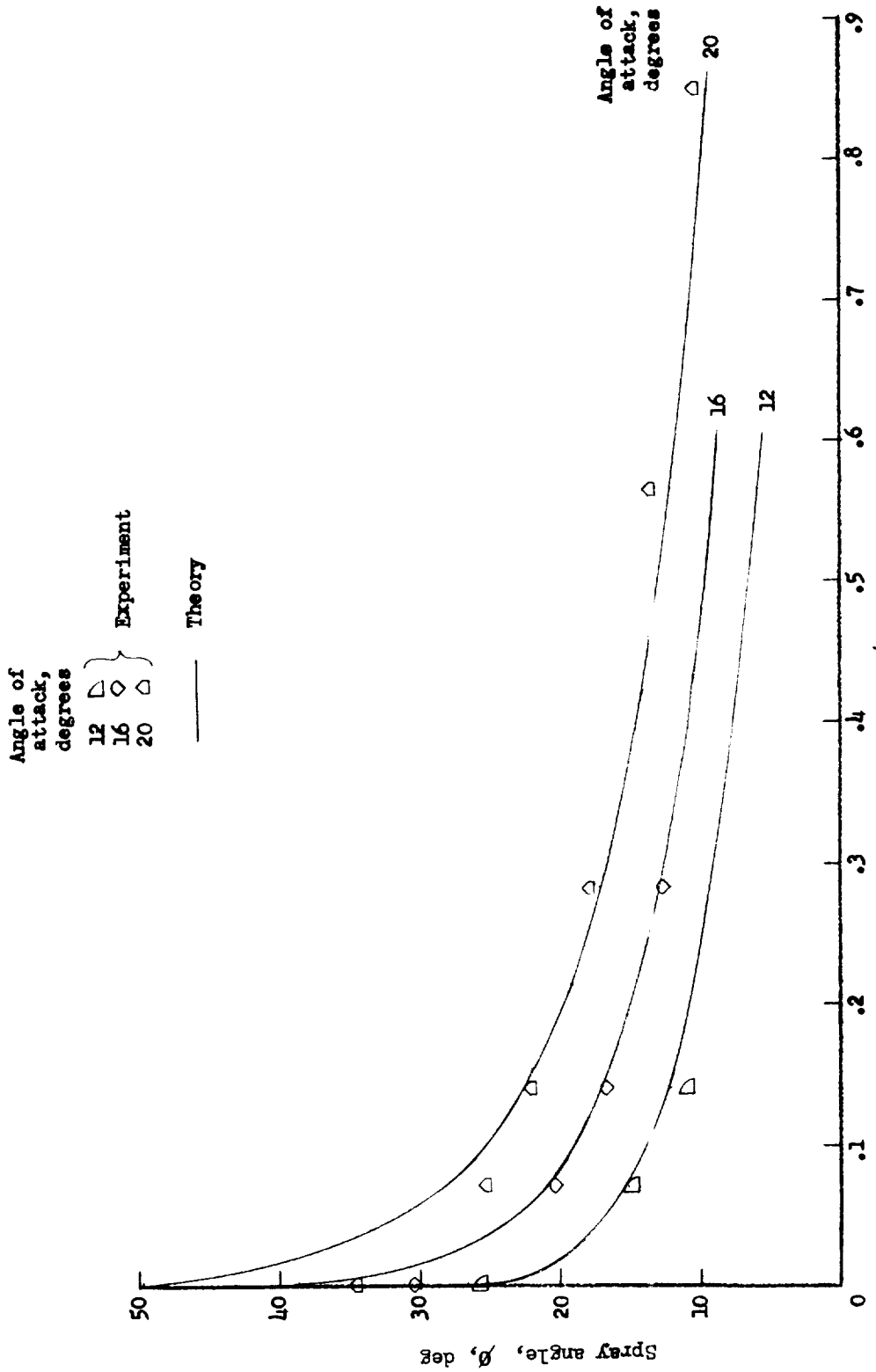

(a) Aspect-ratio-1 hydrofoil.

Figure 17.- Comparison of theoretical and experimental spray angles.

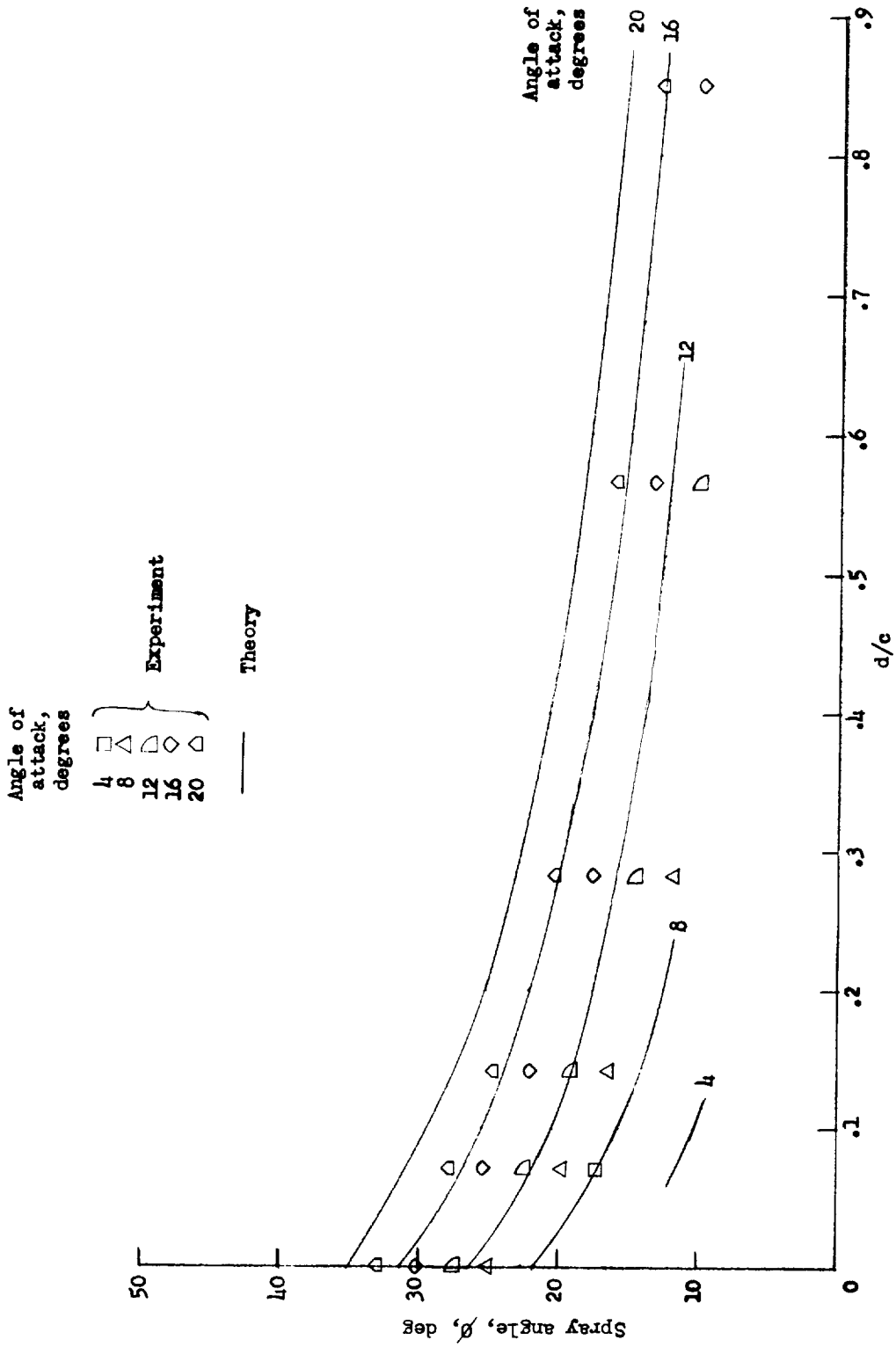

(b) Aspect-ratio-3 hydrofoil.

Figure 17.- Concluded.

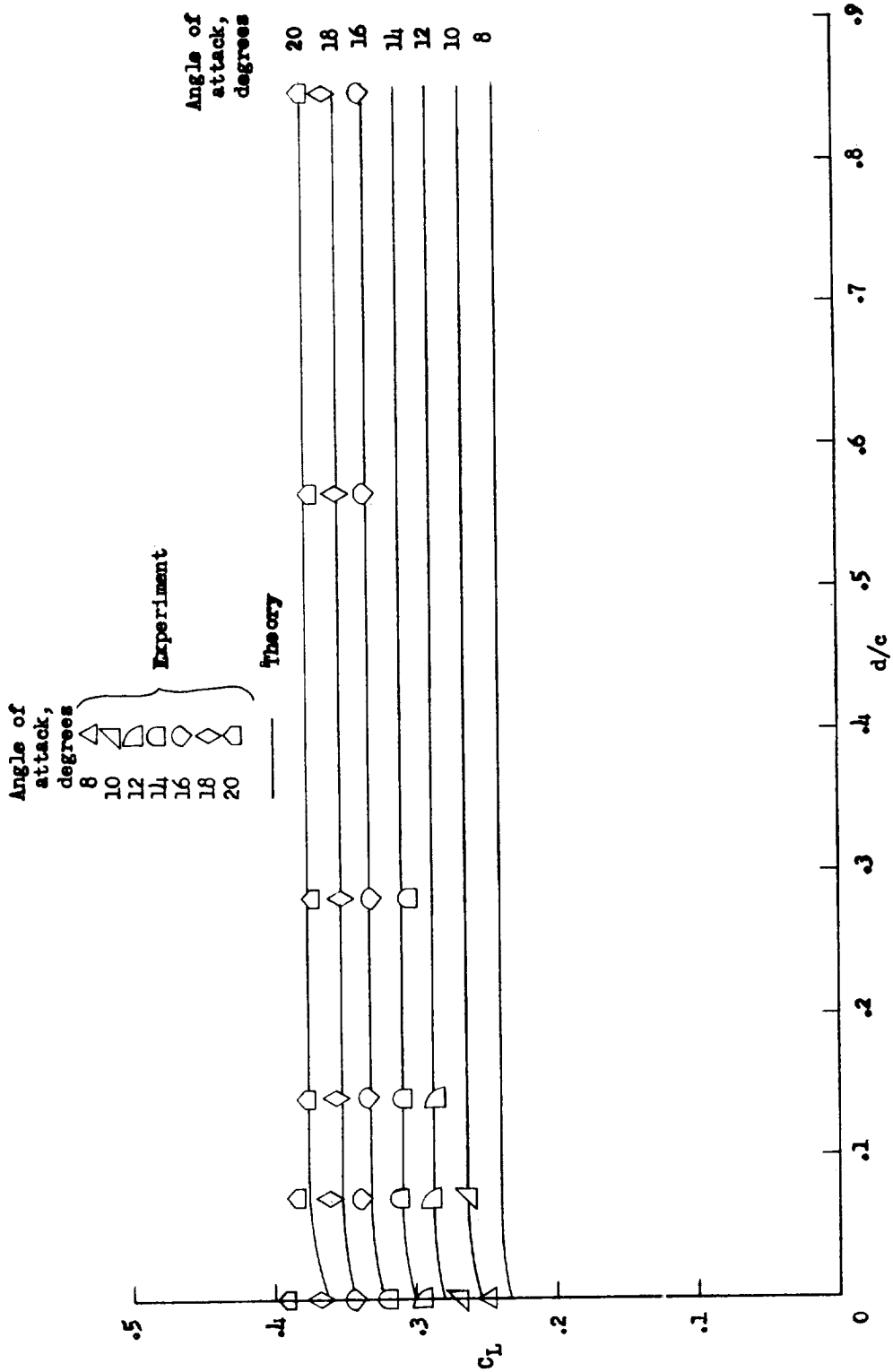

(a) Aspect-ratio-1 hydrofoil.

Figure 18.- Comparison of theoretical and experimental lift coefficients.

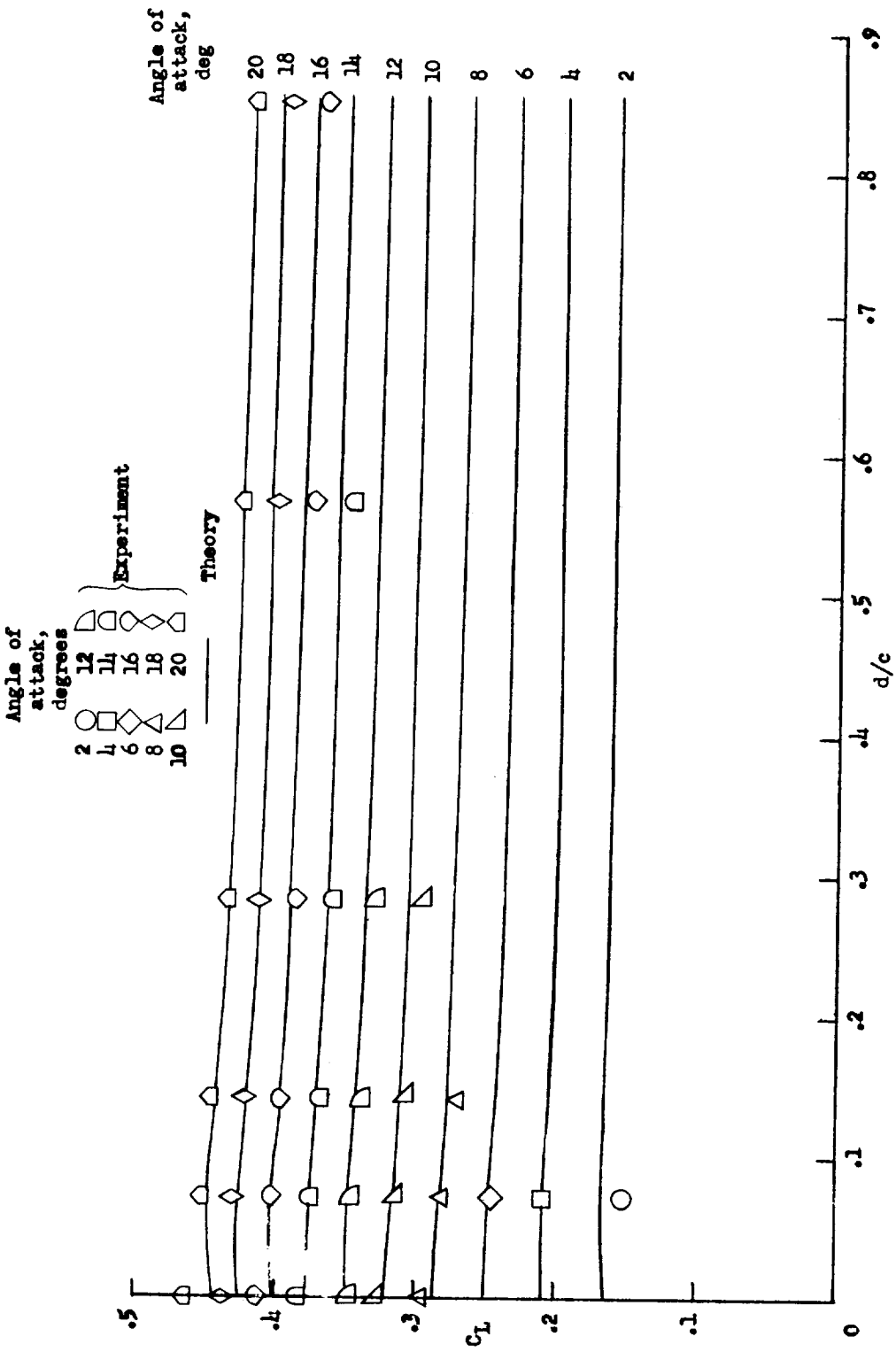

(b) Aspect-ratio-3 hydrofoil.

Figure 18.- Concluded.

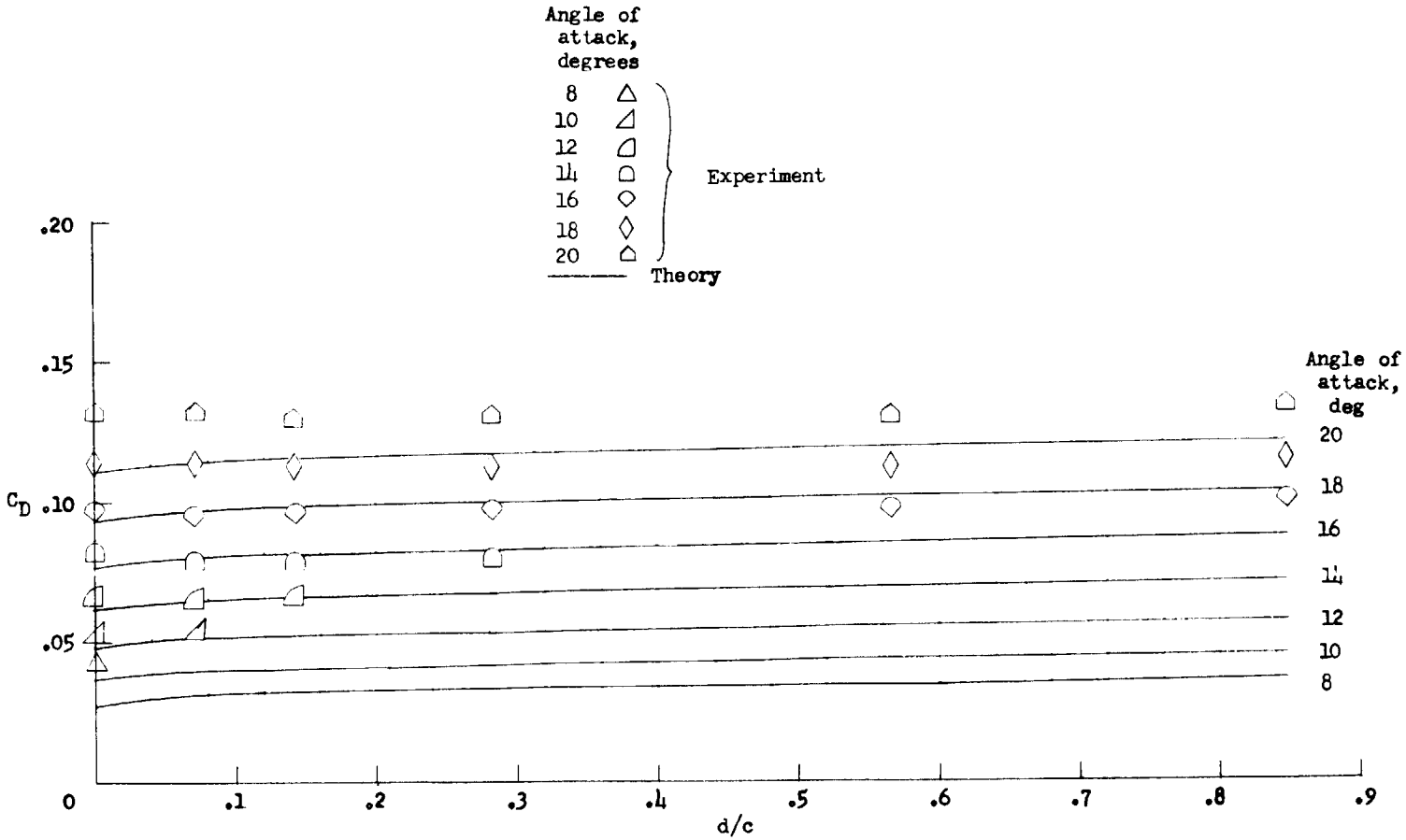

(a) Aspect-ratio-1 hydrofoil.

Figure 19.- Comparison of theoretical and experimental drag coefficients.

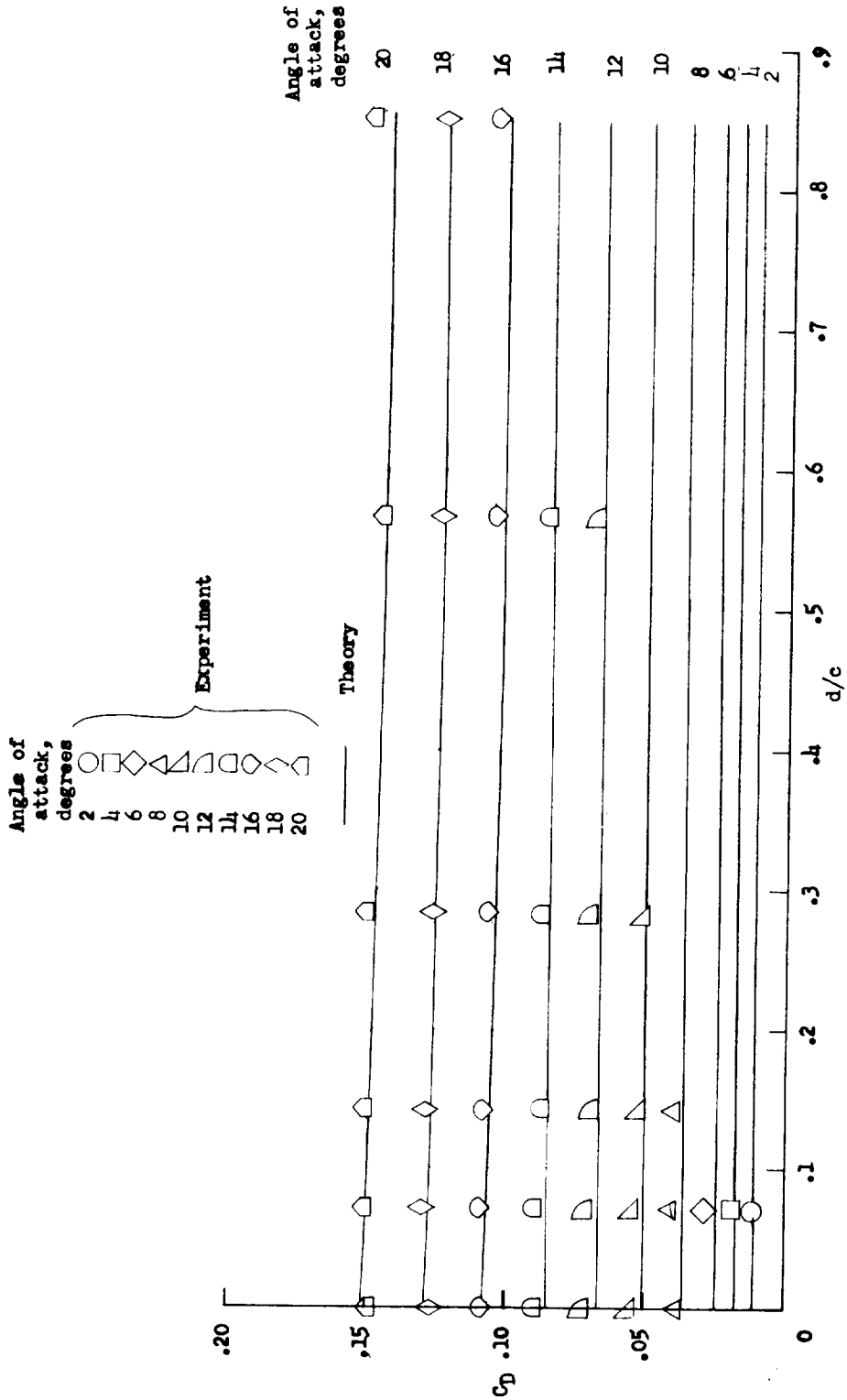

(b) Aspect-ratio-3 hydrofoil.

Figure 19.- Concluded.

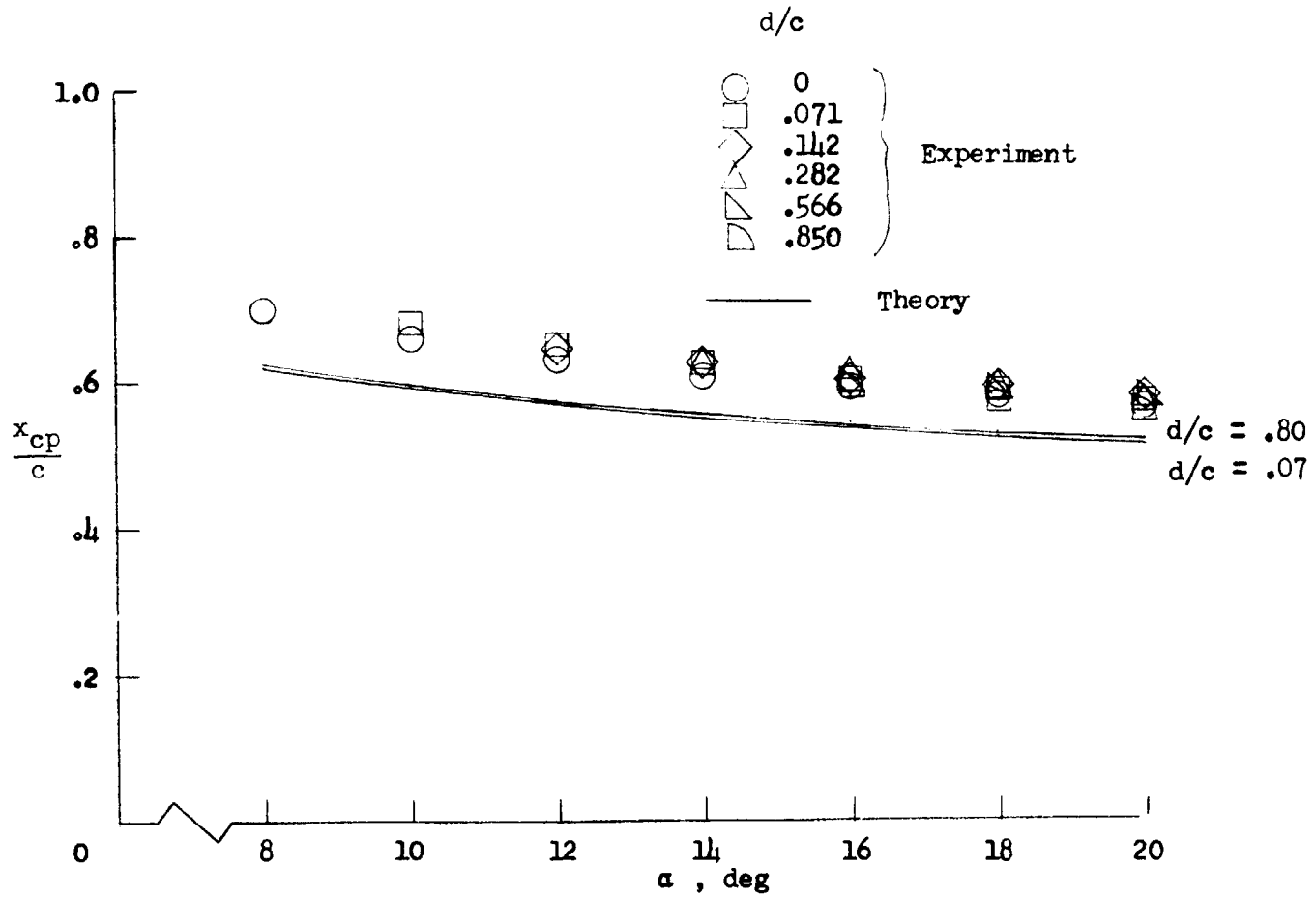

(a) Aspect-ratio-1 hydrofoil.

Figure 20.- Comparison of theoretical and experimental center-of-pressure—chord ratios.

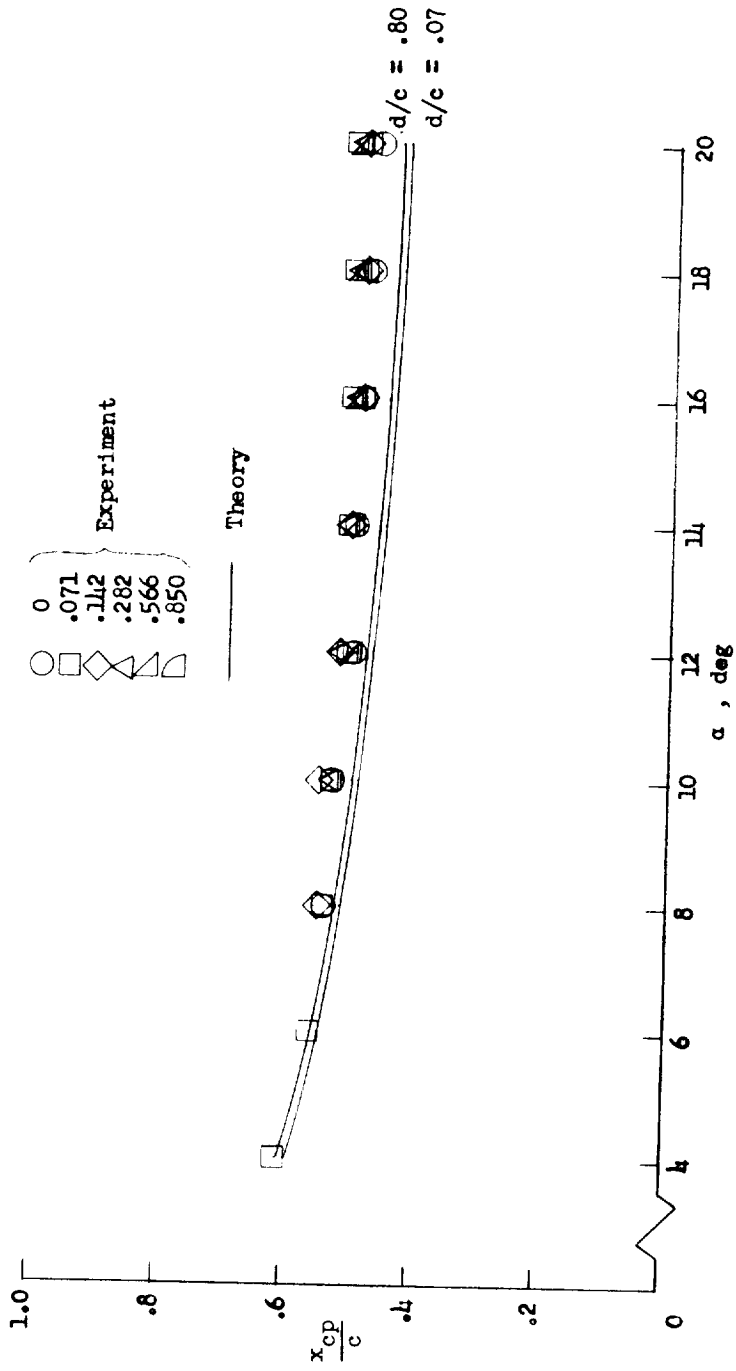

(b) Aspect-ratio-3 hydrofoil.

Figure 20.- Concluded.

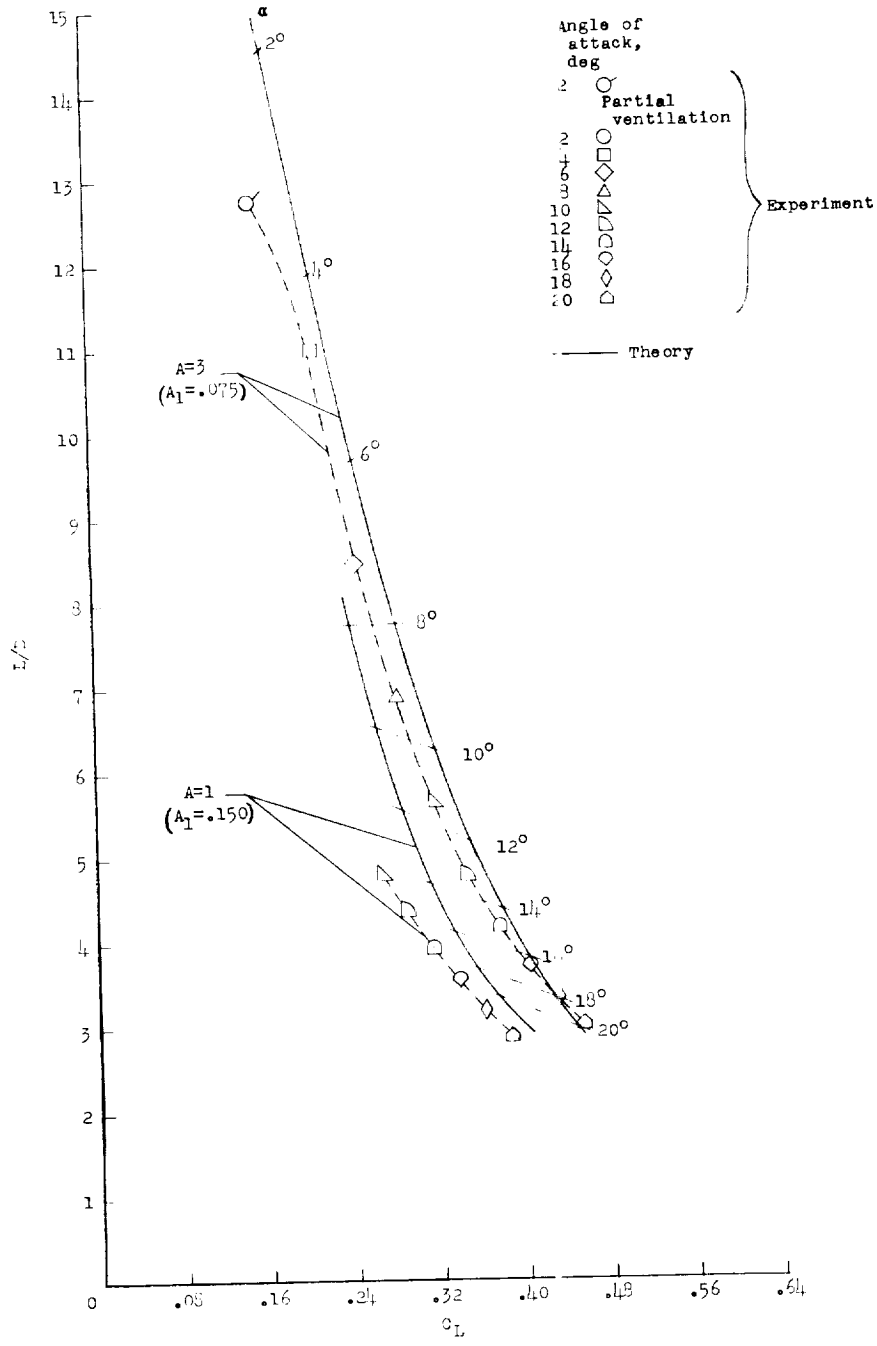

(a) d/c = 0.071.

Figure 21.- Comparison of theoretical and experimental lift-drag ratios for aspect-ratio-1 and aspect-ratio-3 hydrofoils.

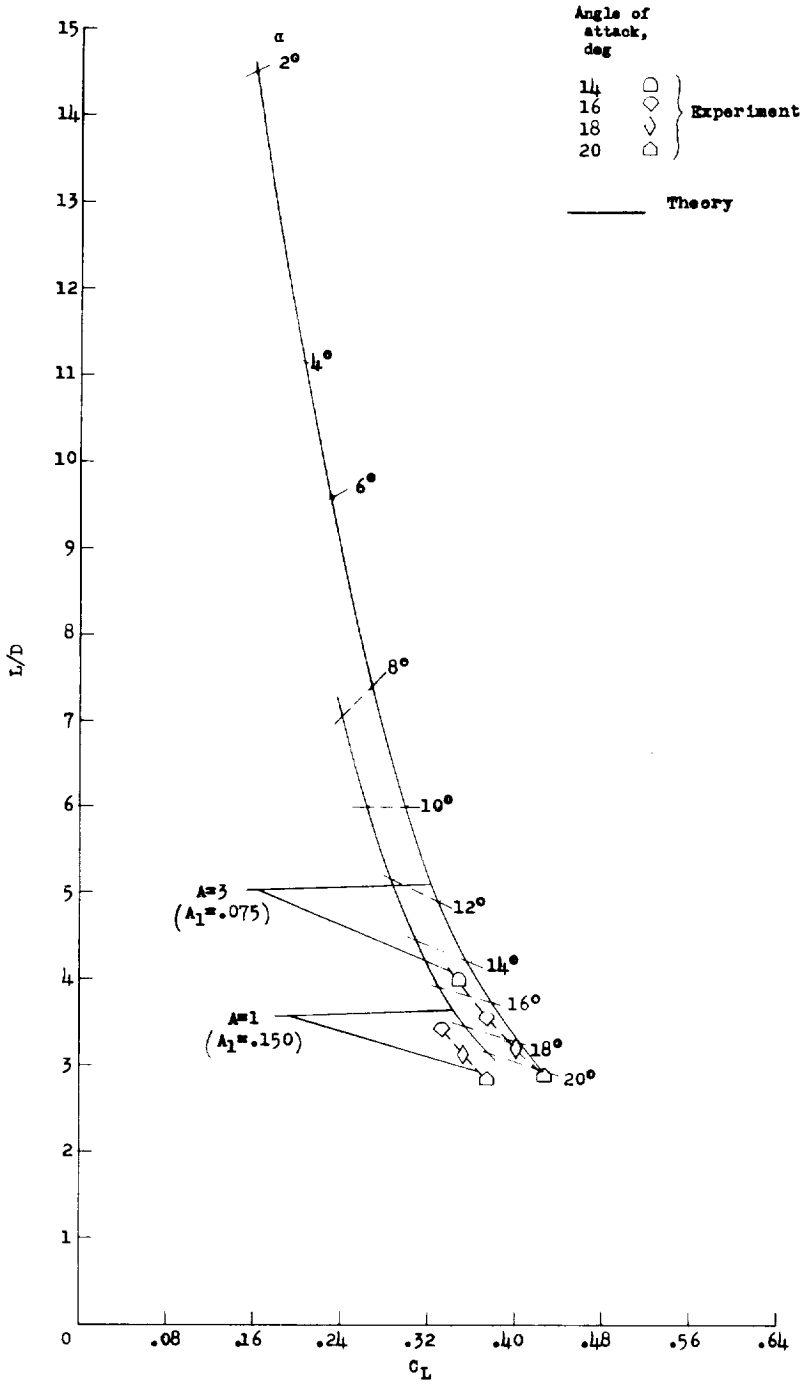

(b) d/c = 0.566.

Figure 21.- Concluded.

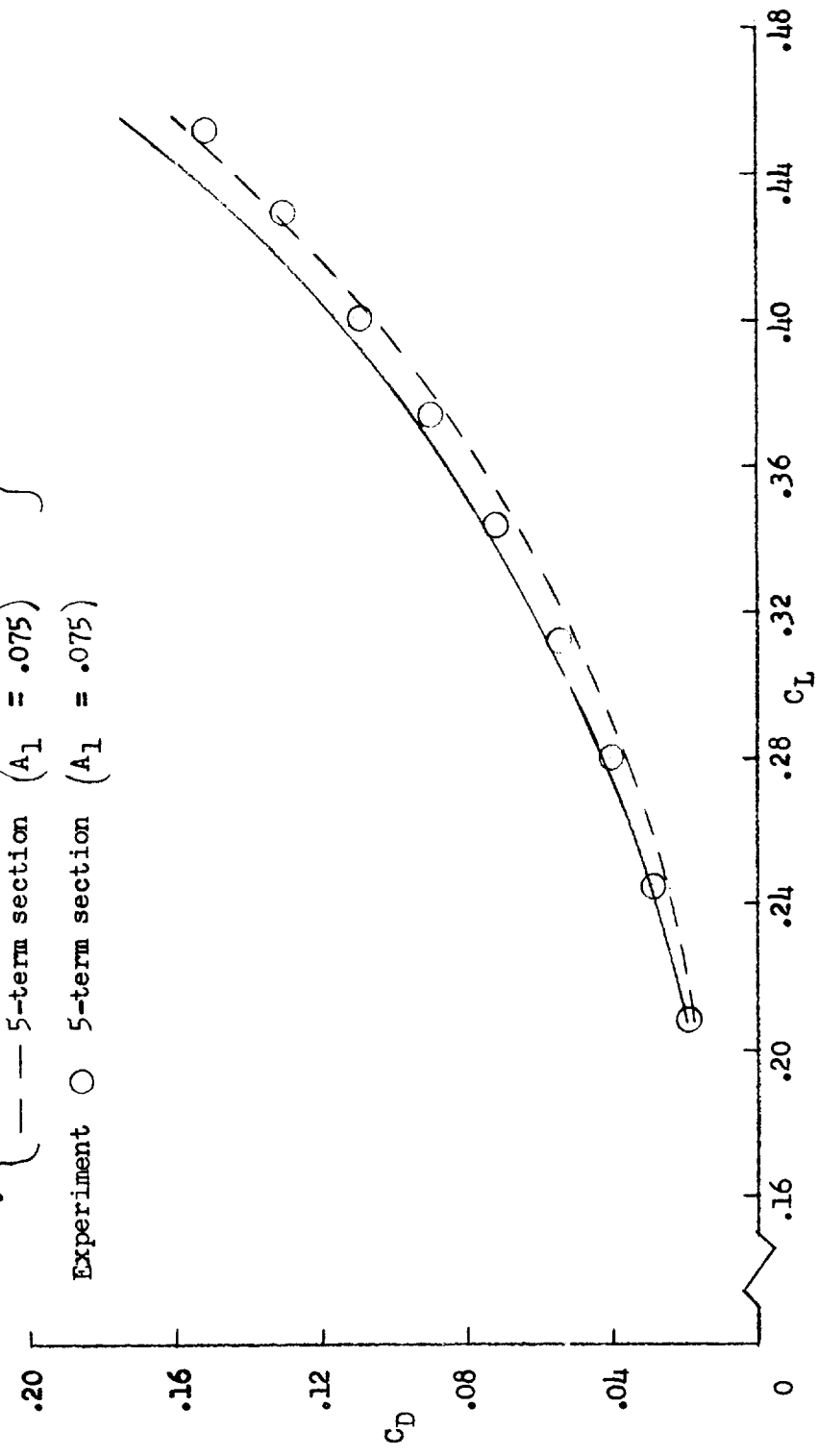

Figure 22.- Comparison of drag coefficients of a Tulin-Burkart hydrofoil with drag coefficients of a five-term hydrofoil. d/c = 0.071; A = 3.